SANDIA REPORT

SAND95-0596 • UC-721
Unlimited Release
Printed May 1997

Hydraulic Fracturing Tests in Anhydrite Interbeds in the WIPP, Marker Beds 139 and 140

W. R. Wawersik, L. W. Carlson, J. A. Henfling, D. J. Borns, R. L. Beauheim, C. L. Howard, R. M. Roberts

Prepared by
Sandia National Laboratories
Albuquerque, New Mexico 87185 and Livermore, California 94550

Sandia is a multiprogram laboratory operated by Sandia Corporation, a Lockheed Martin Company, for the United States Department of Energy under Contract DE-AC04-94AL85000.

Sandia National Laboratories

SF2900Q(8-81)

Issued by Sandia National Laboratories, operated for the United States Department of Energy by Sandia Corporation.

Available to DOE and DOE contractors from
Office of Scientific and Technical Information
P.O. Box 62
Oak Ridge, TN 37831

Prices available from (615) 576-8401, FTS 626-8401

Available to the public from
National Technical Information Service
U.S. Department of Commerce
5285 Port Royal Rd
Springfield, VA 22161

NTIS price codes
Printed copy: A04
Microfiche copy: A01

SAND95-0596
Unlimited Release
Printed May 1997

Distribution
Category UC-721

Hydraulic Fracturing Tests in Anhydrite Interbeds in the WIPP, Marker Beds 139 and 140

W. R. Wawersik, L. W. Carlson,
and J. A. Henfling
Geomechanics Department

D. J. Borns
Geophysics Department

R. L. Beauheim
Geohydrology Department

Sandia National Laboratories
P. O. Box 5800
Albuquerque, NM 87185-0751

C. L. Howard
RE/SPEC Inc.
Albuquerque, NM 87110

R. M. Roberts
INTERA Inc.
Albuquerque, NM 87102

Abstract

Hydraulic fracturing tests were integrated with hydrologic tests to estimate the conditions under which gas pressure in the disposal rooms in the Waste Isolation Pilot Plant, Carlsbad, NM (WIPP) will initiate and advance fracturing in nearby anhydrite interbeds. The measurements were made in two marker beds in the Salado formation, MB139 and MB140, to explore the consequences of existing excavations for the extrapolation of results to undisturbed ground. The interpretation of these measurements is based on the pressure-time records in two injection boreholes and several nearby hydrologic observation holes. Data interpretations were aided by post-test borehole video surveys of fracture traces that were made visible by ultraviolet illumination of fluorescent dye in the hydraulic fracturing fluid. The conclusions of this report relate to the upper- and lower-bound gas pressures in the WIPP, the paths of hydraulically and gas-driven fractures in MB139 and MB140, the stress states in MB139 and MB140, and the probable in situ stress states in these interbeds in undisturbed ground far away from the WIPP.

Acknowledgments

This project was performed over a four-year period with the dedicated and conscientious help of numerous individuals. The authors express their particular thanks to S. Y. Pickering and J. R. Trone, Sandia National Laboratories, for quality assurance support and for the review of the Standard Operating Procedures; C. Mewhinney, Sandia National Laboratories, for advice and reviews concerning pressure safety and materials handling; M. Carriaga, Westinghouse Electric Corp., for machining straddle packer components; D. Parrish, Westinghouse Electric Corp., for drilling support; R. L. Rascon, RE/SPEC Inc., for running borehole video cameras, and M. Fort and W. Stensrud, INTERA Inc., for help in logging core, participating in hydraulic fracturing experiments, and maintaining an INTERA data acquisition system for hydrologic testing. The authors also thank T. Doe and J. Lorenz for a careful review and L. Cleland-Ortiz for help during the preparation of this report.

TABLE OF CONTENTS

1. Introduction 1
2. Background 1
3. Objectives 2
4. Test Locations 3
5. Description of Marker Beds 5
6. Test Description and Procedures 11
7. Hydraulic Fracturing Tools 14
    Packers, Instrumentation, and Data Acquisition 14
    Pre-Test System Evaluations 15
8. Chronology of Combined Hydrologic and Hydraulic Fracturing Tests 16
9. Results 21
    Hydraulic Fracturing Data 21
    Pressure Response in Hydrologic Observation Boreholes 25
    Post-Test Visual Fracture Observations 26
10. Discussion 28
11. Summary and Conclusions 32
12. References. 34
Appendix A -Depths of Interbed Boundaries and Hydraulic Fracturing Intervals 39
Appendix B -Core descriptions, MB139 and MB140 41
Appendix C - Schematics of Hydraulic Fracturing Tools 51
    Figure C1 - Assembly drawing of single-zone, 2-packer systems used for hydraulic fracturing tests in MB139. 52
    Figure C2 - Assembly drawing of two-zone, 3-packer systems used for hydraulic fracturing tests in MB140. 53
    Figure C3 - Schematic of system plumbing for hydraulic fracturing tests in Room C1 54
Appendix D - System Compliance Data 55
    Table D.1 - Packer pressure, p_p, and linear dilatometer travel, d. 56
    Table D.2 - Interval pressure, p_s, and linear dilatometer travel, d. 57
    Table D.3 - Interval pressure, p_s, and linear dilatometer travel, d. 58
    Table D.4 - Packer pressure, p_p, and linear dilatometer travel, d. 58
    Table D.5 - Upper interval pressure, p_{su}, and linear dilatometer travel, d. 59
    Table D.6 Lower interval pressure, p_{sl}, and linear dilatometer travel, d. 60
    Table D.7 - Combined upper and lower interval pressure, p_s, and linear dilatometer travel , d. 60
Appendix E - Instrumentation and Calibration Data 61

List of Figures

Figure 1 - Plan view of WIPP with WIPP Experimental Area. 4
Figure 2a - Hydraulic fracturing and hydrologic test holes in Room C1 - Plan view 5
Figure 2b - Hydraulic fracturing and hydrologic test holes in Room C1 - cross-section. 5
Figure 3a - Borehole pattern of Figure 2 and satellite boreholes for post-test fracture observations. Dashed circle represents hypothetical front of axisymmetric hydraulically driven fracture initiated in test hole C1X05. 6

Figure 3b - Schematic cross-sections with orientations of post-frac observation boreholes shown in Figure 3a. 6
Figure 4 - Characteristic lithologic zones in idealized section of MB139 (after Borns, 1985)..... 8
Figure 5a - Photograph of 0.3 m (1 ft) diameter core taken from MB139 in G-drift - Zones II and III..... 9
Figure 5b - Photograph of 0.3 m (1 ft) diameter core taken from MB139 in G-drift - Zone IV... 10
Figure 6 - Pressure-time and flow rate-time records of single-cycle hydraulic fracturing test in MB139, borehole C1X10. 21
Figure 7 - Pressure-time and flow rate-time records of four-cycle hydraulic fracturing test in MB139, borehole C1X05. 22
Figure 8 - Pressure-time and flow rate-time records of six-cycle hydraulic fracturing test in MB140, borehole C1X05. 24
Figure 9 - Pressure-time data demonstrating borehole responses to post-frac pressure injection test in MB139, borehole C1X05. Injection pressure: 11.62 MPa. See Figure 2 for borehole locations..... 25
Figure 10 - Borehole video records showing fluorescent dye and fluid/gas bubbles associated with hydraulic fractures. (a) Borehole C1X06, MB140 with two well-defined subhorizontal fracture traces, (b) borehole C1X12, MB140 exhibiting two of a set of multiple subhorizontal fractures, (c) borehole C1X12, MB139 with pronounced local (channel) flow along a distinct subhorizontal fracture, and (d) borehole C1X06, MB140 with trace of a subvertical fracture. Note: height of images is 1.1 cm (0.44 in)..... 28

1. Introduction

The Waste Isolation Pilot Plant, Carlsbad, NM (WIPP), is being developed by the Department of Energy (DOE) to demonstrate the safe geological disposal in rock salt of radioactive waste resulting from the defense programs of the United States. A part of the WIPP Technology Development Activities are the Hydrological and Thermostructural Programs. A subset of these activities addresses the consequences of gas generation in disposal rooms in the Salado formation, and specifically, experimental evaluations of analyses concerning the gas pressurization of anhydrite interbeds such as Marker Bed (MB) 139 (Davies et al., 1990; Davies, 1991). To accomplish this, complementary hydraulic fracturing and hydrologic tests were conducted in MB139 and in the deeper MB140. Considerable variability was recorded in the measured formation (pore) pressures and permeabilities in MB139 one to two meters (3-6 ft) below the repository horizon, and to a lesser extent, some 6 m (20 ft) below the floor of the experimental area in the WIPP. The observed variability suggested a strong influence of subhorizontal networks of preexisting partially and fully healed fractures. Additionally, it was deemed possible that MB139 had been altered by the influence of nearby excavations (Stormont et al., 1987; Stormont, 1990a; Beauheim et al., 1991, 1993a). Because MB140 is located approximately 17 m (50 ft) deeper than MB139 (Holt and Powers, 1984), there was a possibility that MB140 was sufficiently less disturbed to serve as a virgin analog of MB139 and other anhydrite interbeds in the vicinity of the repository horizon.

The work that is presented in this report is based on a detailed test plan prepared in 1991 (Wawersik and Beauheim, 1991) and adhered to with only very minor changes. Preliminary results of the combined hydrologic and hydraulic fracturing tests in MB139 were published in 1993 (Beauheim et al., 1993b). The following account provides the first comprehensive description of all hydraulic fracturing measurements. The interpretation of these data benefited greatly from recent post-fracturing (post-frac) borehole observations that became available during a systematic drilling program. The hydrologic measurements made before and after hydraulic fracturing will be alluded only to the extent that they are relevant to the discussion of hydraulic fracture propagation. The hydrologic analyses and interpretations themselves will be addressed in a separate report.

2. Background

The WIPP facility is located in a bedded salt formation approximately 655 m (2,150 ft) below the ground surface. The underground development is separated into the north area, which is an experimental area, and the south area, where the disposal rooms are located. The local stratigraphy contains numerous horizontal layers of anhydrite and clay, as well as halite containing various impurities. Of particular note is a nonsalt layer called Marker Bed 139 immediately below the disposal horizon. MB139 (described in detail by Borns, 1985, and by Holt and Powers, 1984) is a nominally 1 m (3 ft) thick anhydrite layer 1 to 2 m (3-6 ft) below the disposal level (Krieg, 1984; Stormont, 1990b). MB139 is important because it is predicted to be a high-permeability conduit for gas that is generated in storage rooms. As gas pressure in individual storage rooms rises, gas is expected to break through a disturbed, partially fractured salt layer into MB139 (Davies et al., 1990). Subsequent gas flow within MB139, away from the gas source, coupled

with the predicted storage capacity of the anhydrite layer is calculated to limit the maximum possible gas pressure in the storage rooms. The lateral persistence of MB139 also suggested that gas leaving the repository horizon would spread out, but remain in this well-defined horizontal layer.

The analytical foundation of the foregoing predictions entails numerous two-dimensional, coupled analyses of gas and brine flow (Davies et al., 1990; Davies, 1991). Virgin in situ stress conditions and permeabilities used in calculations, in turn, are based on a considerable number of measurements throughout the WIPP horizon (Wawersik and Stone, 1985, 1989; Beauheim et al., 1991, 1993a; Stormont et al., 1991). There are, nevertheless, several uncertainties, some of which are to be addressed by the experiments in this report: (1) Large variability of formation (pore) pressure, permeability, and brine mass collected in drillholes in MB139 leave open the possibility that MB139 was not in the virgin state. This suggestion is consistent with the observation that stress field perturbations in rock salt, and therefore, also along salt-interbed boundaries, appear to propagate much farther than in hard elastic rock (Wawersik and Stone, 1989). (2) Computations implied but did not prove that relatively high gas pressures might open and/or connect partially open, partially healed preexisting fractures in anhydrite. (3) Analyses that existed at the beginning of this study did not include the effects of developing new fractures in MB139 which could (i) remain in the marker bed or (ii) propagate vertically out of the interbed. The latter scenario would be likely if the horizontal in situ principal stress in anhydrite, a nearly elastic material at low and intermediate applied deviatoric stress, were significantly smaller than the overburden stress. Fracture propagation out of the interbed is conceivable also for certain combinations of in situ stress state, fracture length, and fracture resistance (fracture toughness) of MB139 material, the contact between MB139 and the surrounding salt, and of salt above and below MB139 (Gerstle et al., 1996).

All processes leading to increased interbed permeability would tend to reduce the maximum pressure both in MB139 and in the storage rooms. At the same time, higher permeability would enhance the hydraulic connection between different rooms and panels in the repository.

3. Objectives

Hydraulic fracturing (frac) experiments in MB139 and MB140 were designed to answer six specific questions.

- At what fluid pressures will fracturing occur in anhydrite interbeds, especially MB139, both in a potentially disturbed state and in its virgin state?

- If fracturing occurs, would it take place by the opening and interconnection of preexisting, partially healed fractures or would fracturing include the formation of new fractures?

- At what induced (liquid or gas) pressure might fracturing be sustained?

- If fracturing in MB139 involved the development of new fractures, would the fracture process be confined to the anhydrite interbed or would newly created fractures break out of MB139?

- Is the total stress state (matrix stress plus pore pressure) in MB139 and MB140 isotropic or not, and can near-field stress measurements around excavations be used to infer the virgin state of stress in the interbeds?

- What is the magnitude of the smallest principal stress in anhydrite interbeds, if the stress state is anisotropic?

In order to relate the results of the hydraulic fracturing experiments and the effect of fracturing to the hydrologic properties of MB139 throughout the WIPP, it was essential to combine all frac experiments with pressure buildup and flow measurements both before and after hydraulic fracturing was induced. The details of these flow tests will be described elsewhere. However, it was the goal of these tests to provide:

- Reliable values of formation (pore) fluid pressure,

- Permeabilities and storage capacities of the interbeds before and after hydraulic fracturing causing at least local dilation of preexisting and, possibly, the formation of new fractures, and

- Comparisons of permeability measurements in MB139 relatively near existing excavations with equivalent data in MB140 which was expected to be essentially undisturbed or at least less disturbed than MB139.

4. Test Locations

All tests were performed in Room C1 in the northeast portion of the WIPP experimental area, 642 m (2105 ft) below ground surface. Room C1 lies in one of the least mined areas of the WIPP (Figure 1) where the excavation floor is located approximately 6 m (20 ft) higher above the top of MB139 than the floor of all planned disposal rooms. Both characteristics offered the possibility that the in situ stress field and the properties of ground in and immediately around MB139 and MB140 might be altered less than at any other potential experimental location. The only more remote and possible preferable places would have been along the G-drift towards the northwest corner of the WIPP. The G-drift was precluded, however, because of space limitations and potential effects on other critical measurements.

Hydraulic fracturing tests were conducted in two drillholes, C1X10 and C1X05 (Figure 2). Borehole C1X10 was drilled near the intersection of Room C1 and the drift N1420 to evaluate all test procedures although it was expected that the results obtained might not be representative of the marker beds in their virgin states. More conclusive measurements were to be obtained in borehole C1X05 that was placed within 1.5 m (5 ft) from the north end of Room C1 (Figure 2).

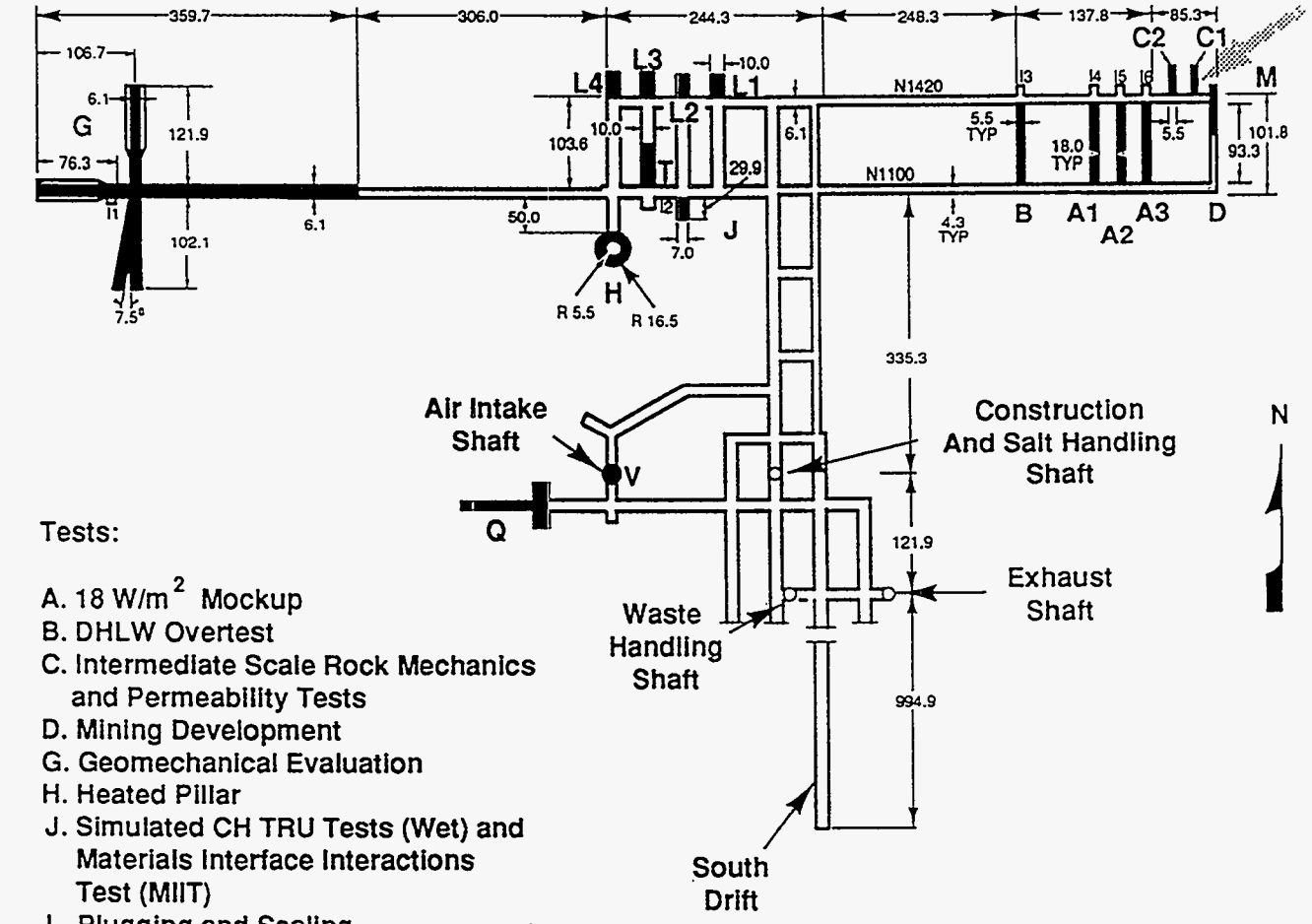

Figure 1 - Plan view of WIPP with WIPP Experimental Area.

Borehole C1X10 was drilled through MB139 only whereas borehole C1X05 penetrated both MB139 and M140. Boreholes C1X10 and C1X05 served as sources and sinks for hydraulic fracturing tests and for pre- and post-frac hydrologic injection and withdrawal experiments. Satellite holes (boreholes C1H05 through C1H07 and C1X06; Figure 2) were put down to support the hydrologic measurements and to trace the paths of the hydraulically induced fractures. Details concerning the depths of the marker beds and the locations of the test intervals are summarized in Appendix A.

Several additional boreholes (C1X07 through C1X13) were drilled after the completion of all tests to obtain supplementary information concerning the character, orientation, extent, and geometry of all hydraulic fractures. The planar area sampled by the latter observation boreholes is indicated by the dashed circle around the injection hole C1X05 in Figure 3a. Borehole C1X13 was planned to reach beyond this circular observation area. Further details concerning the course of the observation holes C1X07 through C1X13 are indicated in Figure 3b.

5. Description of Marker Beds

Marker Beds 139 and 140 are two of a series of siliceous or sulfatic units of the Salado formation located nominally 1.5 m (5 ft) and 19 m (62 ft) below the repository horizon of the WIPP, respectively. These and other interbeds are the result of repeated flooding of the Salado basin followed by evaporite concentration, reworking and intersediment growth. The general characteristics of MB139 have been described by Borns (1985) based on the evaluation of five sets of core from SPDV complex, Room 4 in the WIPP. Accordingly, the approximately 1-m-thick MB139 can be divided into five characteristic zones. The uppermost Zone I includes a distinctive claystone up to several centimeters (inches) thick which is overlain by polyhalitic halite. Undulations of the claystone-halite contact on top of MB139 are 10 to 50 cm (4 to 20 in) in amplitude and 30 to 100 cm (1 to 3 ft) in wavelength.

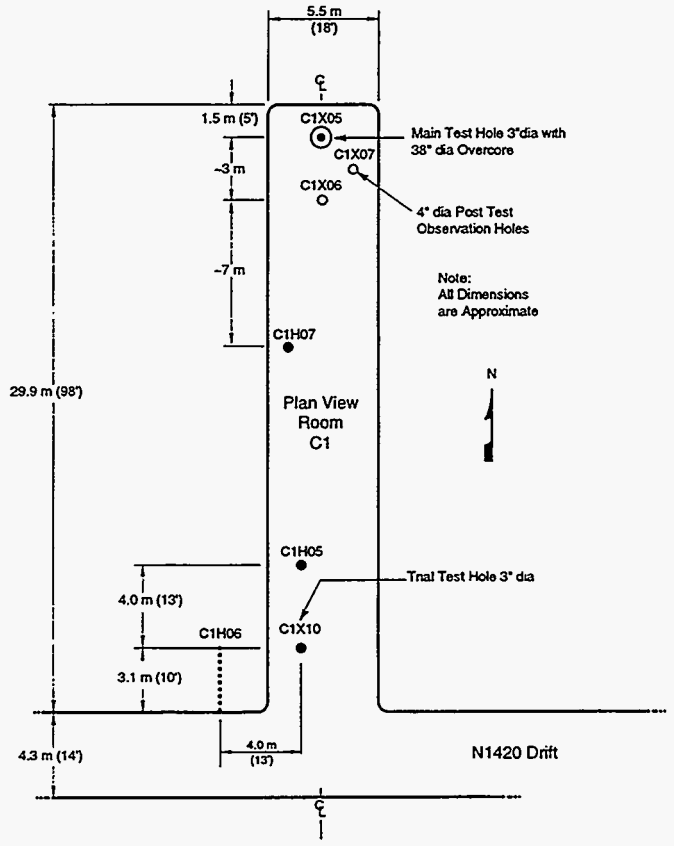

Figure 2a - Hydraulic fracturing and hydrologic test holes in Room C1 - Plan view

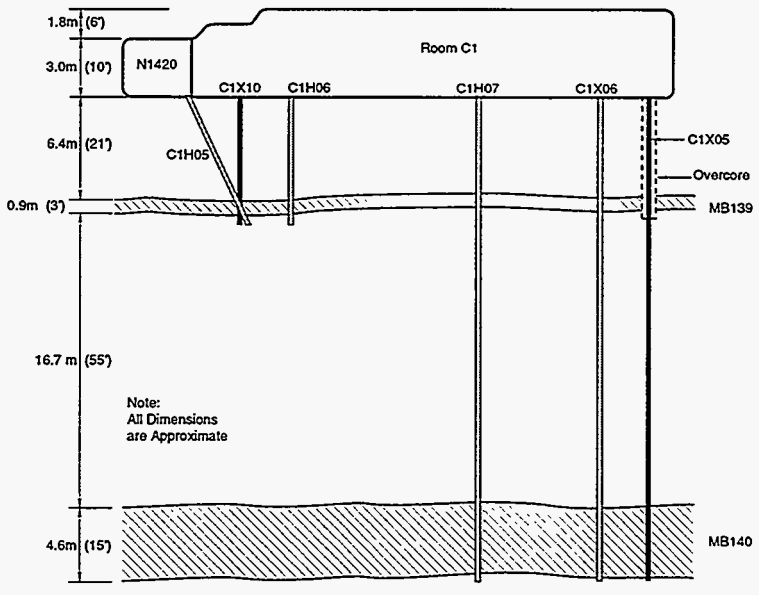

Figure 2b - Hydraulic fracturing and hydrologic test holes in Room C1 - cross-section.

Where Zone I is thin and the claystone is in contact with the polyhalitic anhydrite in Zone II, the claystone infills embayments into the anhydrite. The lower portion of Zone I may be made of interlayered halite, polyhalite, and clay with partially broken hopper and chevron crystals.

A massive polyhalitic anhydrite Zone II is 20 to 30 cm (8 to 12 in) thick and exhibits a distinct spotted appearance. The spots are 1 to 5 mm (0.04 to 0.2 in) in diameter and are formed from radiating clusters of polyhalite. Contorted and undulated stylolite laminae crosscut both anhydrite and polyhalitic anhydrite. Some boreholes in this zone reveal clusters of swallowtail structures and replacement patches of halite.

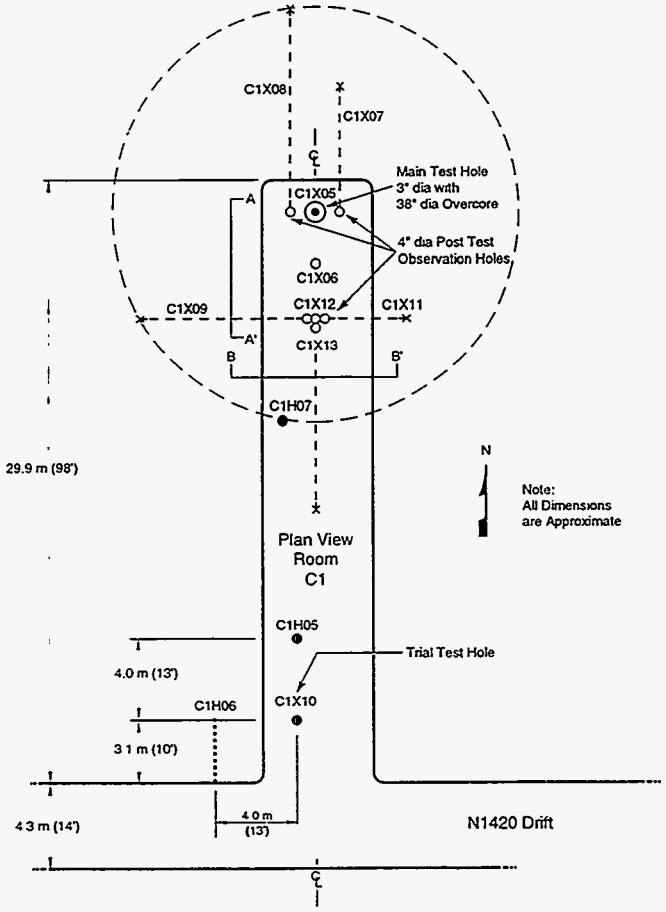

Figure 3a - Borehole pattern of Figure 2 and satellite boreholes for post-test fracture observations. Dashed circle represents hypothetical front of axisymmetric hydraulically driven fracture initiated in test hole C1X05.

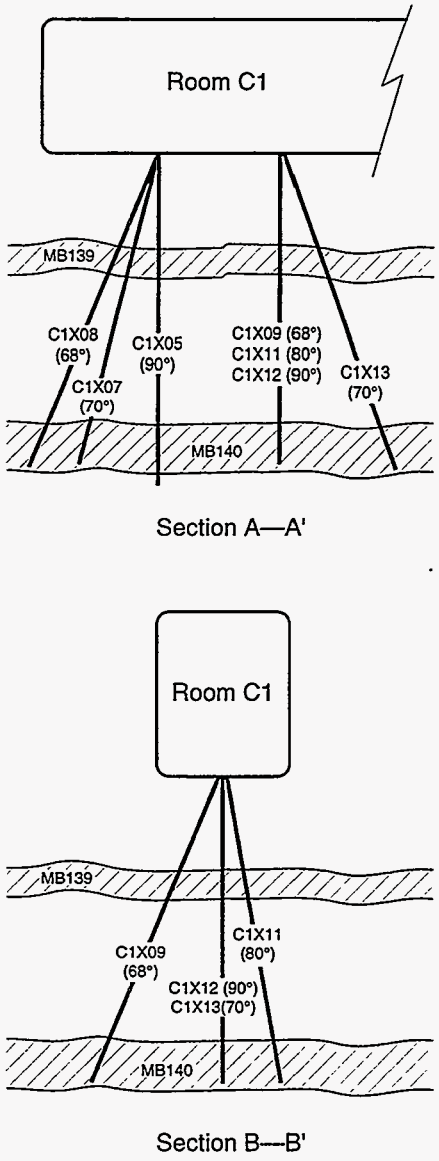

Figure 3b - Schematic cross-sections with orientations of post-frac observation boreholes shown in Figure 3a.

The mixed anhydrite and polyhalitic anhydrite Zone III has a distinct marbled appearance enhanced by a mixture of red and green colors. The lower part of Zone II and especially Zone III contain pervasive sets of subhorizontal fractures. The fractures generally follow the sedimentary layering, but locally cross layering or follow the layering where it has been deformed by sedimentary or diagenetic processes. The fractures in both zones are infilled or partially infilled with halite, but infillings of polyhalite and fine-grained anhydrite are also present. Partial infilling is observed in core and on borehole surfaces regardless of whether they were drilled with brine or air suggesting that the fractures and non-filled porosity are not artifacts of the drilling process.

The laminated anhydrite with halite Zone IV also is 20 to 30 cm (8 to 12 in) thick and characterized by fine laminations of halite and gray-green relict anhydrite. Individual subhorizontal laminae are 1 to 2 cm (0.4 to 0.8 in) thick. Anhydrite occurs either as multiple laminae with thin (1 mm, 0.04 in) interlaminae of clay or as laminae in halite. Anhydrite laminae in halite exhibit pull-apart structures, and as in Zone II, are infilled partially by halite. While the set of partially open fratures are not observed in Zone IV as in Zones II and III, Zone IV exhibits numerous planes of weakness and partings.

The bottom contact of Zone V is marked by a gray-blue clay zone. Much of the clay was often lost during drilling and core removal. Where the section is recovered intact, the clay band appears to be about 1 to 2 cm (0.4 to 0.8 in) thick.

A typical (idealized) schematic cross-section of MB139 is shown in Figure 4. The general features observed by Borns (1985) in Room 4 have been confirmed by core observations (Appendix B) made as part of the present hydrologic and hydraulic fracturing measurements that entailed coring in Room C1 and in the G-drift in the eastern portion of the WIPP experimental area (Figure 1). The main Zones II to IV are particularly recognizable in the photographs of 0.3 m (1 ft) diameter core taken in the G-drift and included as Figures 5a and 5b. Variations from the Zone description above primarily pertain to considerable variations in zone thicknesses. For example, Zone I in the injection borehole C1X05 was 55 cm (22 in) thick compared with a combined thickness of Zones II-IV of only 25 cm (10 in) in C1H07. All cores exhibited core breaks along local lithologic contrasts and partially or fully healed subhorizontal fractures, especially in Zones II and IV.

It was stated earlier that MB140 is located some 17 m (55 ft) below MB139, and therefore, offered the possibility of evaluating the flow and fracturing characteristics of a characteristic interbed that was close to its virgin state, undisturbed by existing WIPP excavations. Core inspections of three boreholes in Room C1, boreholes C1X05, C1X06, and C1H07 (Appendix B) established that MB140 was formed by the same depositional cycle as MB139 except that MB140 represents not only one but two cycles of flooding. As a result, MB140 is approximately 4.2 m (13.8 ft) thick and contains two distinct clay zones separating the entire interbed into an upper, approximately 3.4 m (11.2 ft) thick sequence closely resembling Zones I-IV in MB139 and another 0.8 m (2.6 ft) thick lower sequence including Zones II-V. Zones III and IV in the upper sequence are considerably thicker than their counterparts in MB139. Apparent local changes are reflected in substantial thickness variations of Zones II and

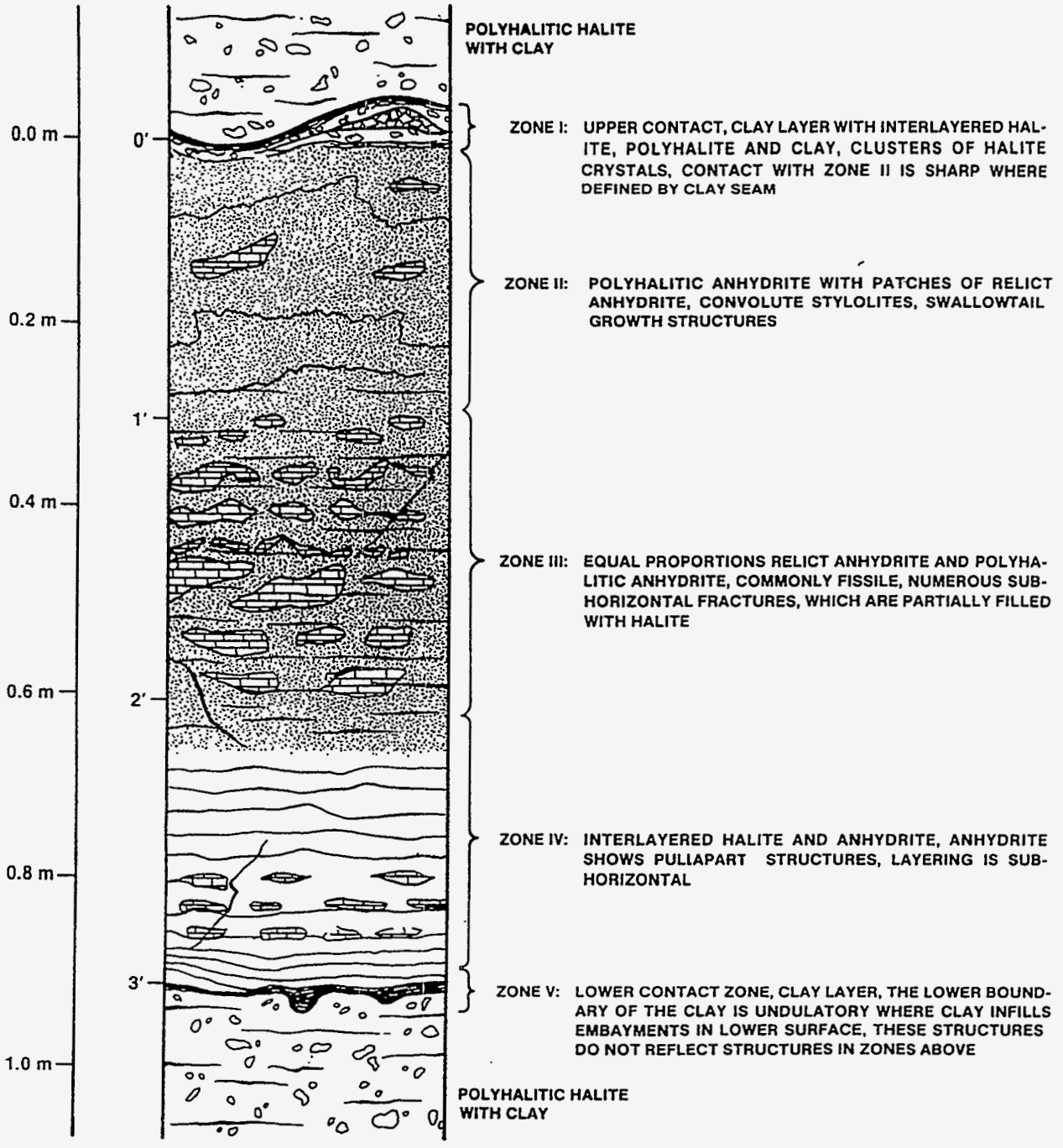

Figure 4 - Characteristic lithologic zones in idealized section of MB139 (after Borns, 1985).

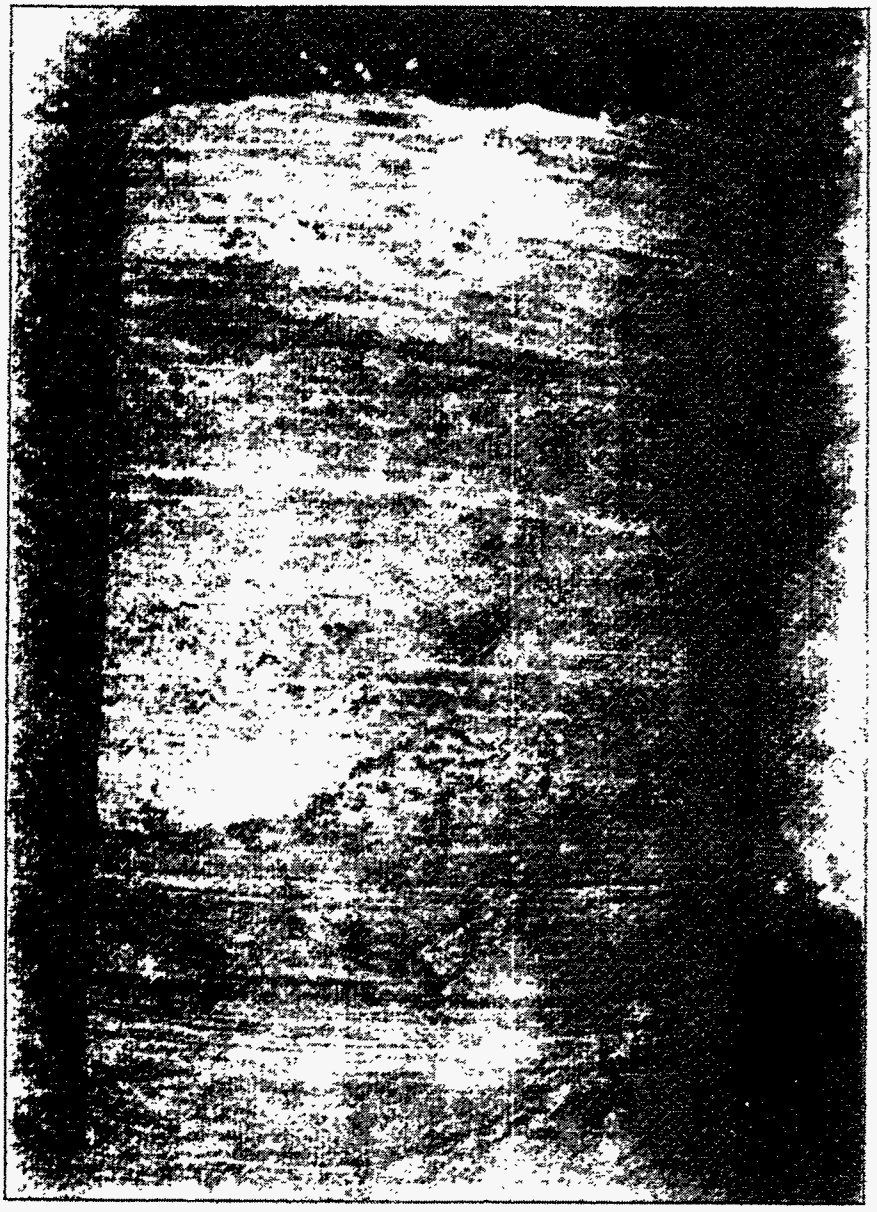

Zone II

Zone III

Figure 5a - Photograph of 0.3 m (1 ft) diameter core taken from MB139 in G-drift - Zones II and III

Zone IV

Figure 5b - Photograph of 0.3 m (1 ft) diameter core taken from MB139 in G-drift - Zone IV.

III in the lower sequence. In fact, Zone II and III were absent in borehole C1H07. Instead, the two clay zones were separated only by a 0.6 m (2 ft) thick layer of massive gray anhydrite.

The equivalence of MB139 and MB140 was principally determined from mesoscopic observations of core and borehole television logs. Considering the objectives of fracturing tests in the two interbeds, all core comparisons were guided by five key questions relevant to the project: (1) What are the main lithological and structural properties of the two marker beds and is any portion of the thicker MB140 an acceptable analog of the much thinner MB139? (2) How uniform are the marker bed characteristics among the test boreholes in Room C1, and how do they compare with the "typical" description of Borns (1985)? (3) Are there features such as depositional contrasts, open or healed fractures, etc., that might influence or even dictate the direction of propagation of hydraulically or gas-driven fractures? (4) Is there evidence of excavation-induced damage to suggest that measurements during flow or hydraulic fracturing measurements might not apply to virgin ground? Finally, (5) are there petrographic or structural features, as opposed to potential excavation effects, that might cause asymmetrical growth of fractures around the injection holes? Clearly, preexisting partially or fully healed fractures and breaks of core along some of these features indicated the presence of preexisting weakness planes that could influence the paths of hydraulically induced fractures unless the latter were determined solely by strong differences between the maximum and minimum in situ principal stresses.

6. Test Description and Procedures

The combined hydraulic fracturing-hydrologic tests consisted of a trial experiment in MB139 and a main test series in MB139 and MB140. All measurements were conducted in the two 7.6 cm (3 in) diameter boreholes, C1X10 and C1X05 (Figure 2). The trial test was designed to evaluate the test procedures, to provide a preliminary indication of the preferred path(s) of hydraulically induced fractures, and to obtain estimates of the local formation (pore) pressure and permeability of MB139. This experiment also determined whether a straddle-packer system with single packers, i.e., without additional guard packers at each end, was adequate for isolating borehole sections in anhydrite with partially healed preexisting fractures. Finally, the trial experiment was used to evaluate post-frac observations of fracture paths using an existing borehole video camera and observations in two nearby 10 cm (4 in) diameter observations holes. Because borehole C1X10 was located next to the intersection of two drifts, it was anticipated that mining-induced disturbances at that location might be severe.

The main hydraulic fracture and hydrologic measurements in MB139 and MB140 were located in drillhole C1X05 that was cored in sections, first through and to approximately 1.3 m (4 ft) below MB139 and subsequently, after completion of the first set of measurements, to approximately 1.3 m (4 ft) below MB140. To minimize pore-fluid drainage and attendant changes to the formation, testing commenced with the shortest possible delay (≤12 hours) after drilling. Each set of measurements included:

I. Tool emplacement and pressure buildup phase

Accurate volume measurements during hydrologic tests in tight formations require that the compliance of the test system is known, low, and nearly constant. To accomplish this, air in the test zones was minimized by pouring some 15 L (4 gallons) of fracturing fluid into the borehole. At that point, the straddle packer was lowered and set at approximately 7 MPa (1,000 psi) pressure. Most of the remaining air in the tubing between the test zone, the high-pressure pump, and the control console was removed by means of a vacuum pump before fracturing fluid was added. As soon as possible (1 to 4 hours), the interval pressure was increased to 5.5 MPa (800 psi) to accelerate the establishment of pressure equilibrium with the formation pore pressure. Based on past experience in MB139, the formation pressure was expected to lie between 6 and 11 MPa (870-1,600 psi; Beauheim et al., 1991, 1993a). As the interval pressure rose with time, the packer pressure was adjusted if necessary to be at least 2 MPa (290 psi) above the interval pressure to prevent that fluid would leak by the packer elements.

Following similar procedures, packers were installed in the hydrologic observation holes (Figure 2). A detailed chronology of all experimental activities will indicate later the sequence in which the hydraulic fracturing and hydrologic observation boreholes were drilled and packed off.

In some cases, the phase of building up pressure in the intervals between the packer elements had to be interrupted in order to fix leaks in the tubing trains or around

some packers. As a result, the pressure buildup phase was especially protracted at the beginning of the measurements in borehole C1X05, MB140. Small, but persistent, fluid losses (<1 mL per day) ultimately required that the packer elements in that borehole were modified by the addition of soft rubber sleeves to close off passageways between the packers and the rough borehole wall.

II. Hydrologic testing

Hydrologic testing was started once the pressure in the test zones between packer elements had stabilized, indicating that the borehole pressures were approximately in equilibrium with the formation pore pressure. Hydrologic tests before hydraulic fracturing consisted of injection tests at pressure varying from 0.5 to 1.6 MPa (75 to 230 psi) above the formation pressure. When possible, the injection pressures were held constant.

Each suite of hydrologic tests before hydraulic fracturing was concluded with measurements of the packer and interval compliances in the injection borehole. The method to do so was established in pre-test system evaluations using a double-acting hydraulic actuator to increase or decrease the system pressures in steps between 0.07 and 0.35 MPa (10-50 psi). The associated fluid volumes were calculated from the displacements of the actuator piston.

III. Hydraulic fracturing

Hydraulic fracturing tests consisted of one to six individual pressure cycles. Each cycle was carried out at an approximately constant flow rate of 4.5-5.7 L/min (1.2-1.5 gpm) with the exception of cycle four in borehole C1X05, MB140, when the flow rate was lowered to 0.19 L/min (0.05 gpm). The total fluid injection volume per pressure cycle was between 1 L (0.3 gal) and 31 L (8.2 gal), and each shut-in lasted about eight minutes. After that, the interval pressure was brought back to the initial (formation) pressure and backflow of fluid into the injection hole measured to estimate the amount of fluid lost into the rock. Additional details concerning the procedures of completing the hydraulic fracturing tests are listed in the (Standard) Operating Procedures for these measurements (Wawersik, 1991, 1992, 1993).

Once hydraulic fracturing was completed, the pressure in the injection interval was lowered below the original formation pressure to recover as much injection fluid as possible. The interval was then isolated to reestablish pore pressure equilibrium between the injection zone and the formation.

IV. Post-frac Hydraulic testing

Hydrologic tests of the type performed during phase II were combined with constant-pressure withdrawal experiments in order to compare Marker Beds' permeabilities before and after the creation of hydraulically induced discrete fractures. Because fracture aperture is sensitive to the total normal stress across a fracture (Brown,

1987), post-hydraulic fracturing hydrologic tests also identified the effect of injection pressure on fracture conductivity.

V. Post-test visual fracture observations

Visual fracture observations were important in order to determine the paths of the hydraulically induced fractures and to interpret the pressure-time records of the hydraulic fracturing tests. Visual observations were based on core inspections and on the reviews of borehole video surveys with white and ultraviolet light illumination. The size of the video camera with black light, however, required that the 7.6-cm (3-in) diameter injection boreholes C1X10 and C1X05 be reamed to 10.2-cm (4-in) diameter. Efforts for delineating the geometry of the hydraulic fractures and possible effects of nearby excavations, especially Room C1, also motivated the drilling of the seven additional observations boreholes C1X07 through C1X13 shown in Figure 3.

The effective lengths of the hydraulic fracturing intervals varied between 0.7 m (2.3 ft) in borehole C1X10, MB139 and 1.3 m (4.3 ft) in C1X05, MB140. In all cases, the decision was made to prevent fluid from penetrating into the upper and lower contacts of the interbed with the adjacent salt. Fracture propagation along these contacts might have provided no data concerning the fracturing conditions within MB139 or MB140.

The core observations discussed previously indicated that the upper third of MB140 would be a good analog of MB139. To initiate hydraulic fracturing in the top part of MB140, the borehole through MB140 was segmented by means of a three-packer tool that permitted pressure to be controlled independently between the top and middle and between the middle and bottom packers, respectively. Subdividing MB140 also offered a possibility to monitor how hydraulically induced fractures might grow away from and vertically along a borehole in this relatively thick unit. Two dominant clay layers that were mentioned in the lithologic description of MB140 were located in the lower interval in MB140.

Using different packer tools, efforts were made to isolate the top one third from the rest of MB140 in the hydrologic observation boreholes C1X06 and C1H07. The packer locations in C1H07, indeed, turned out to be equivalent to the packer placement in C1X05. On the other hand, the tool was placed higher in C1X06. As a result, later hydraulic fracturing data showed that the lower interval in C1X06 included a portion of the active test zone of the upper interval in C1X05.

All hydraulic fracturing and hydrologic experiments were performed by injecting Chevron Mineral Seal Oil 38, a thin hydraulic oil with a viscosity of 2.2 cp at 40° C, as reported by the manufacturer. Low-compressibility liquid, as opposed to gas, was used to generate pressure-time signatures with high contrast in order to delineate the onset of hydraulic fracture development, monitor fracture growth, and resolve pressure variations with time after shut-in. Hydraulic oil also avoided equipment corrosion. Corrosion almost certainly would have led to the loss of flow control during hydraulic fracturing which did not start until several weeks after the straddle packer system, fill lines, pumps, etc., had been filled with test fluid.

Substituting liquid for gas to assess gas-pressurization effects in the interbeds is permissible only if differences in the associated threshold pressures can be estimated and shown to be small. Because anhydrite has a matrix permeability as low as $k = 10^{-21}$, it is generally assumed that the effective permeabilities of anhydrite interbeds, $k=10^{-18}$ to $k=10^{-19}$ m^2 (Davies et al., 1990; Beauheim et al., 1991, 1993a) are dominated by fracture flow. This means that the permeability of the actual flow paths must exceed $k=10^{-18}$ m^2. Computed threshold pressures for gas-brine systems under these conditions are less than 1 MPa (Davies, 1991). Given the oil-water surface tension and viscosity of Mineral Seal Oil 38 published in the manufacturer's specifications, $\sigma = 2.04 \times 10^{-2}$ N/m and $\mu = 2.2$ cp at 40° C, the threshold pressure in corresponding flow measurements and hydraulic fracturing tests was estimated to be less than 0.5 MPa (70 psi). This value was based on an extreme upper-bound tortuosity T = 0.25 of dilated fractures where T is the ratio of the length of the fracture system (L) and the length of the actual flow path (L_e). In both cases, the threshold pressures were deemed to be sufficiently small to characterize the gas-flow properties by means of liquids, and specifically, measurements with a low-viscosity oil.

7. Hydraulic Fracturing Tools

Packers, Instrumentation, and Data Acquisition

Hydraulic fracturing tests were carried out by means of variations of a conventional two-element straddle packer with stainless steel straddle rod(s) (Wawersik, 1991, 1992, 1993). The inflatable packer elements consisted of 122-cm (48-in) long, 6.45-cm (2-5/8-in) diameter slat-type elements acquired from Baker Service Tools with outer and inner packer tube designations #808 and #801, respectively. The length of the elastomer covers on all packers was 76 cm (30 in). Figure C1 in Appendix C shows the assembly drawing of the tool that was fielded in two sets of combined fluid flow and hydraulic fracturing measurements in MB139. The straddle rod was machined of 2.5-cm I.D. x 3.8-cm O.D. (1.0 x 1.5 in) stainless steel pipe. The length of the straddle rod was selected so that each packer element would be centered over the upper and lower contacts of MB139 whose thickness in the test area varied between 0.8 and 0.95 m (2.6 and 3.1 ft). As usual, the packer ends on the interval side were free to move as the packer elements were pressurized and expanded. One adapter ('sub') of each packer was equipped with a 20.7 MPa (3,000 psi) rupture disk. Additionally, the bottom sub of the tool contained a vent in order to purge the packer from air as it was filled with fluid. The top sub contained ports for separate fluid supply lines to the packers and to the hydraulic fracturing interval between the packers. A third port permitted the installation of a pressure gage for downhole measurements of the interval pressure. A 0.953-cm O.D. x 0.775-cm I.D. (0.375 x 0.305-in) 304 stainless steel supply line to the hydraulic fracturing interval ensured that the interval volume remained nearly constant with time in order to obtain reliable measurements of the formation pressure before flow or hydraulic fracturing tests were initiated. Early test simulations in a steel pipe indicated that this condition could not be maintained with a 23 m (75 ft) long flexible high pressure hose (Aeroquip No. 2781-04, 0.63 cm/0.25 in I.D.) whose internal diameter changed steadily with time.

Figure C2 in Appendix C shows the assembly drawing of the straddle packer configuration that was used in MB140. To control pressure in two zones, the straddle packer in Figure C1 was

modified in four ways. First, a new (middle) sub (part 24) and another sliding sub were built to incorporate a third packer element. Second, a manifold (part 20) was mounted on top of the straddle packer, and third, an adaptor (part 23) was installed into the new (middle) sub in order to feed an additional, independent fluid supply line to the lower interval. Finally, fourth, the straddle rods between the top, middle, and bottom subs were segmented to facilitate the handling of the tool and the process of inserting and lowering it into drillholes at locations with limited headroom. It was mentioned earlier that in one test it became clear that fluid passed between some of the packer covers and the borehole wall even though the packer pressure was 4 MPa (580 psi) greater than the interval pressure. Because the rock formation at the packer location did not contain any preexisting fractures, it appeared that the relatively hard (70 durometer) packer covers did not conform fully to the shape of the test hole. This problem was eventually solved by covering the center 31 cm (12 in) of each 76 cm (30 in) long packer element with a tightly fitting tube of soft (40-45 durometer) neoprene tubing.

Figure C3 in Appendix C shows a schematic of the fluid supply systems for the single- and two-zone straddle packers. The drawing includes the location of the electronic pressure gages used to monitor the packer pressure, the interval pressure at the console, and the interval pressure downhole on top (gage not shown) of the packer system as indicated in Figures C1 and C2. The fluid and pressure source consisted of an air-driven Haskel pump (model GSF-60-6) in parallel with a 19 L (5 gallon) Haskel accumulator (Haskel part no. 5-5-100-1). Combinations of compact pressure transducers of Kulite Semiconductor Products and signal conditioners/readouts of Entran Devices Inc. and Beckman Instruments Co. were used throughout. In the MB140 experiments, the pressures in both the upper and lower straddle packer intervals were measured only at the console because the downhole pressure gage had been damaged during packer installation. Fluid flow during hydraulic fracturing tests was measured by means of flow meters by EG&G Flow Technology, Inc. (models FT4-8NEXB-LEA-5 and FT4-8NESB-LEDS2) covering the flow ranges 0.2-18.9 L/min (0.05-5 gpm). Fluid flow in the range of 1.9-11.4 L/min (0.5-3 gpm) was controlled by means of a Teledyne flow control valve (catalog series 664). Under all other conditions, fluid flow was regulated manually. Further details concerning the instrumentation and instrument calibrations are listed in Appendix E.

Data records were acquired and maintained in two ways. Manual records contained all system compliance measurements, the starting and final conditions of the hydraulic fracturing tests, and the cumulative volumes of fluid that were either injected or collected as backflow after each pressure cycle or pump. The pressure histories of pressure buildup measurements and of injection, withdrawal, and hydraulic fracturing tests were recorded on parallel sets of computers maintained by the Sandia Geomechanics and Geohydrology Departments. The equipment of the Geohydrology Department was primarily used in all pre- and post-hydrofrac hydrologic experiments. The data-acquisition software used by Geomechanics personnel was the commercial software package LabTech Notebook. Data were stored on floppy disks.

Pre-Test System Evaluations

The straddle packer, control panel, and data acquisition system used were evaluated in extensive pre- and post-test leak and flow tests in a steel pipe before they were fielded in the

WIPP. The steel pipe contained an adjustable pressure relief valve to simulate fluid flow from the interval between pressurized packer elements in situ. Pre-test measurements in the pipe established the lowest differential pressure (1.1 MPa/160 psi) between the packers and the interval(s) of the two- and three-packer systems before fluid started to leak between the packer covers and the pipe. Combinations of pre- and post-test observations also established friction losses (≤0.2 MPa/30 psi) in the supply lines as a function of tubing length and flow rate into MB139 and MB140 at flow rates up to 19 L/min (5 gpm). Finally, the packer compliance, the interval compliances, and the coupling between changes in packer and interval pressures were measured to separate extraneous changes in system volume from fluid flow into the formation during permeability tests in very tight strata (Appendix D). Volume changes in compliance measurements were made by means of a construction type, double-acting hydraulic actuator (Enerpac, model RR1010). For reference, pre-test calculations indicated that a formation permeability of 10^{-19} m^2 would result in 16 mL of fluid flow per day in a constant-pressure injection test following a pressure step of 1 MPa (145 psi).

Other system checks were performed immediately before each hydraulic fracturing test. In particular, with the test intervals isolated, fracturing fluid was circulated through the console to adjust the flow regulator and to flush the pressure lines between the pump and the supply tubing to the test intervals downhole.

8. Chronology of Combined Hydrologic and Hydraulic Fracturing Tests

Table 1 provides a detailed chronology of the combined hydrologic and hydraulic fracturing tests.

Table 1 - Chronology of combined hydrologic and hydraulic fracturing tests by test location, date, and activity. Dates in parentheses denote elapsed times in days used in all hydrologic test records. Pressures p_u and p_l denote upper and lower interval pressures.

Test I.D.	*Date*	*Activities*	*Comments*
C1X10/ MB139	11/11/91 (315)	**Drill** into **MB139**	3.5 L of brine accumulation during 15 hours after drilling
	11/12/91 (316)	Complete drilling through MB139 and install straddle packer. Initiate pressure buildup measurements	
	11/15/91 (319)	Increase interval pressure from 5.52 MPa to 6.5 MPa for injection test 1. Test duration 30 min.	Fluid injection volume 456 mL
	11/19/91 (323)	Increase interval pressure from 6.5 MPa to 9.0 MPa for injection test 2. Test duration 50 min.	Fluid injection volume 1252 mL
	11/26/91 (330)	Increase interval pressure from 6.76 MPa to 9.14 MPa for injection test 3. Stop injection after 6 hours.	Fluid injection volume 7831 mL
	12/5/91 (339)	**Perform single-cycle hydraulic fracturing test** starting at 7.33 MPa.	11.5 L of fluid injected into formation
	12/6-12/13/91 (340-347)	Monitor fluid backflow at interval pressure ≥7.52 MPa	5.68 L of fluid recovery after 16 hours and 8.76 L of fluid recovery 90 hours after test
	12/13/91- 1/16/92 (347-381)	Lower interval pressure to 7.4 MPa and monitor pressure recovery to 9.60 MPa	
	1/16/92(381)	**Drill** observation hole **C1H05** through MB139	
	1/17/92 (382)	Set and inflate packer system in C1H05.	
	1/21/92 (386)	**Drill** observation hole **C1H06** through MB139. Drillhole inclination: 70° from horizontal	
	2/6/92 (403)	Increase interval pressure from 7.56 MPa to 9.0 MPa for post-frac injection test. Test duration ≈ 4 hours.	Fluid injection volume 32 L
	3/18/92 (443)	Reduce interval pressure from 7.98 MPa to 6.40 MPa. Test duration ≈ 6 hours.	Fluid volume withdrawn 7940 mL
	3/18-5/7/92 (443-491)	Monitor recovery of interval pressure to 7.68 MPa.	
	5/7/92 (491)	Terminate testing in C1X10 but maintain packer tools in boreholes C1X10, C1H05 and C1H06 until completion of tests in nearby drillhole C1X05.	

Test I.D.	*Date*	*Activities*	*Comments*
C1X05/ MB139	6/25/92 (176)	**Drill C1H07** through MB139	
	6/26/92 (177)	Install straddle packer	
	6/29/92 (180)	**Drill C1X05** through MB139	
	6/30/92 (181)	Set straddle packer in MB139, and initiate pressure buildup measurement	
	8/4/92 (217)	Start injection test 1 with pressure increase from 9.18 MPa to 10.34 MPa. Test duration ≈ 2 hours two hours at final pressure of 9.744 MPa	
	8/4/92 (217)	Increase injection pressure from 10.16 to 10.18 MPa	
	8/5/92 (218)	Stop injection test 1 at 10.16 MPa	Fluid injection volume 50.33 mL
	8/10/92 (223)	Start injection test 2 with pressure increase from 9.30 MPa to 10.23 MPa.	
	8/20/92 (233)	Terminate injection test 2 at 10.18 MPa	Fluid injection volume 37.96 mL
	9/11/92 (255)	Increase packer pressure	
	9/16/92 (260)	**Conduct hydraulic fracturing test** starting from 9.55 MPa.	Peak pressure 16.71 MPa
	9/17/92 (261)	Reduce interval pressure to	Pressure in C1H07 drops from 9.28 to 8.08 MPa over 4 hrs, then increases
	9/18/92 (262)	Shut in test interval	
	9/29/92 (273)	**Drill C1X06** through MB139 and set packer	Pressure in C1X05 drops gradually from 9.28 MPa. Pressure in C1H07 unchanged
	10/1/92 (275)	Set and pressurize packer	
	11/17/92 (322)	Start post-frac injection test with pressure increase from 9.30 MPa to 10.40 MPa	Noticeable pressure increase only in C1X06
	12/1/92 (336)	Increase injection pressure to 11.62 MPa Test duration: ≈ 2 hours	Fluid injection volume 2786 mL Pressure response in all boreholes
	1/13/93 (379)	Start constant pressure withdrawal test with pressure decrease from 9.10 MPa to 8.14 MPa	
	1/27/93 (393)	Shut in withdrawal test at 8.25 MPa	
	3/11/93 (464)	Terminate testing in C1X05, MB139. Shut in interval and monitor pressure buildup to 8.84 MPa	

Test I.D.	*Date*	*Activities*	*Comments*
C1X05/ MB140	6/14/93 (164)	**Drill C1X05** through MB140	
	6/15/93 (165)	Set 2-zone straddle packer in C1X05	
	6/22/95 (172)	Depressurize packer to fix leak	
	7/7/93 (188)	Depressurize packer to repair leak	
	7/27-29 (208-210)	Remove straddle packer from C1X05 and replace packer elements	
	8/30/93 (242)	Pull and reinstall C1X05 tool after covering packer elements with soft rubber sleeves	
	9/1/93 (244)	Depressurize packer to fix leak	
	9/23/93 (266)	Increase pressure in upper interval from 5.93 to 8.64 MPa	
	10/21/93 (294)	Start constant-pressure injection test with pressure increase from 9.38 MPa to 10.55 MPa	
	10/22/93 (295)	Increase injection pressure to 10.71 MPa	Note: change in upper interval pressure p_u causes increase $\Delta p_l \leq 0.2$ MPa
	11/1/93 (305)	Shut in injection test and isolate upper interval of C1X05	
	11/2/93 (306)	Reconnect C1X05, upper interval again	
	11/22-23/93 (326-327)	**Start hydraulic fracturing tests** in C1X05 from upper and lower interval (reference) pressures p_u=10.69 and p_l=11.70 MPa	Note: starting pressures in C1X06, p_u=8.53 MPa, p_l=11.84 MPa. Pressures in C1H07 unreliable because of leaks
	11/23/93 (327)	Complete hydraulic fracturing tests in C1X05	
	12/1/93 (335)	Increase lower interval pressures in C1H07	Note absence of pressure changes in C1X05 and C1X06.
	12/9/93 (343)	Pull and reinstall tool in C1H07	Note small pressure drops in upper and lower intervals of C1X05 (Δp_u=0.8 MPa, Δp_l=0.06 MPa) ; note also (i) minor pressure drops in lower and upper intervals of C1X06 and (ii) lack of connection between lower and upper intervals in C1X06 indicated by different pressures, p_u= 8.44, and p_l=11.69 MPa at that time.
	12/13/93 (347)	Pull tool from C1H07	Note similar but more pronounced pressure changes as on day 343 (Δp_u=1.93 MPa, Δp_l=0.34 MPa in C1X05)
	12/15/93 (349)	Reinstall tool in C1H07	Pressure variations up to 4.8 MPa in upper and lower intervals to day 354 had no noticeable effect on pressures in C1X05 and C1X06

Test I.D.	*Date*	*Activities*	*Comments*
C1X05/ MB140 (con't.)	12/23-25/93 (357-359)	Tool repairs resulted in several short-term pressure drops up to 10 MPa (to approximately 1 MPa) in upper and lower intervals of C1H07	C1H07 pressure fluctuations reflected in C1X05 and C1X06 as before.
	1/10/94 (375)	Start constant-pressure injection test by pressure increase from 11.71 to 12.27 MPa with gradual drop to 11.91 MPa	Note small, gradual pressure increase in lower interval of C1X05 (Δp_l=0.07 MPa). Strong and minor responses in C1X06, lower and upper intervals. No noticeable response in C1H07.
	1/20/94 (385)	Briefly increase injection pressure from 11.91 to 12.66 MPa, then shut in injection test	Note immediate response in C1H07, lower interval, Δp_l=0.1 MPa.
	2/15/94 (411)	Start constant-pressure withdrawal test from 11.59 to 11.11 MPa	Little to no response in lower interval, C1X05. Almost immediate response, Δp_l= 0.46 MPa, in C1X06. Response in upper interval C1X06 stronger than in lower interval C1X05. Very small delayed response in C1H07.
	3/1/94 (425)	Shut in constant-pressure withdrawal test at 11.10 MPa	
	3/10/94 (435)	Terminate test	Final pressures - C1X05: p_u = 11.61 MPa, p_l= 11.64 MPa; C1X06: p_u= 8.00 MPa, p_l= 11.72 MPa; C1H07: p_u = 9.16 MPa, p_l= 11.58 MPa

9. Results

Hydraulic Fracturing Data

Figures 6 to 8 show the pressure-time curves of the three hydraulic fracturing tests conducted in boreholes C1X10 and C1X05. Following normal practice, the characteristic pressures in each plot are the initial borehole (pore) pressure, p_{on}, the peak (primary and subsequent breakdown) pressure, p_{bn}, the fracture extension pressure before shut-in, p_{en}, and the so-called instantaneous shut-in pressure, p_{sn}, immediately after pumping is stopped and before the pressure declines gradually (often exponentially) with time as fluids leaks off into the formation, and in some cases, slow fracture growth continues (Figures 6 and 7). The second subscript "n" refers to the pressure cycle, e.g., from first to fourth for the test in C1X05, MB139. All of the characteristic pressures and the volumes of fluid injected during each pressure cycle are summarized in Table 2. The interval pressures for the two sets of tests in MB139 were recorded downhole, on top of the straddle packer. The interval pressures listed for hydraulic fracturing in MB140 were taken at the test console, approximately 24 m (80 ft) above the test interval. The latter data have not been corrected for elevation head (<0.2 MPa) and friction losses (<0.2 MPa).

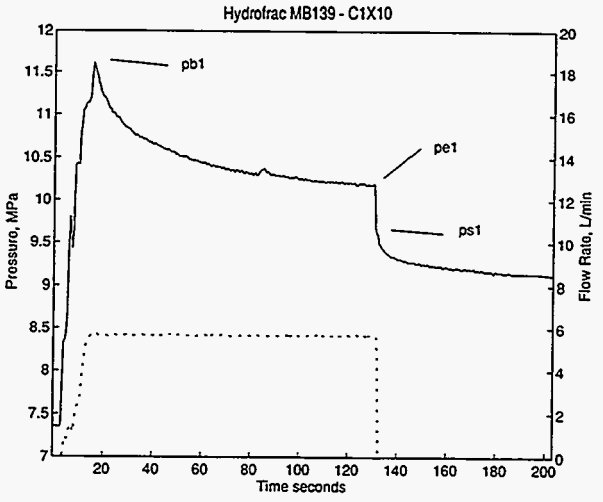

Figure 6 - Pressure-time and flow rate-time records of single-cycle hydraulic fracturing test in MB139, borehole C1X10.

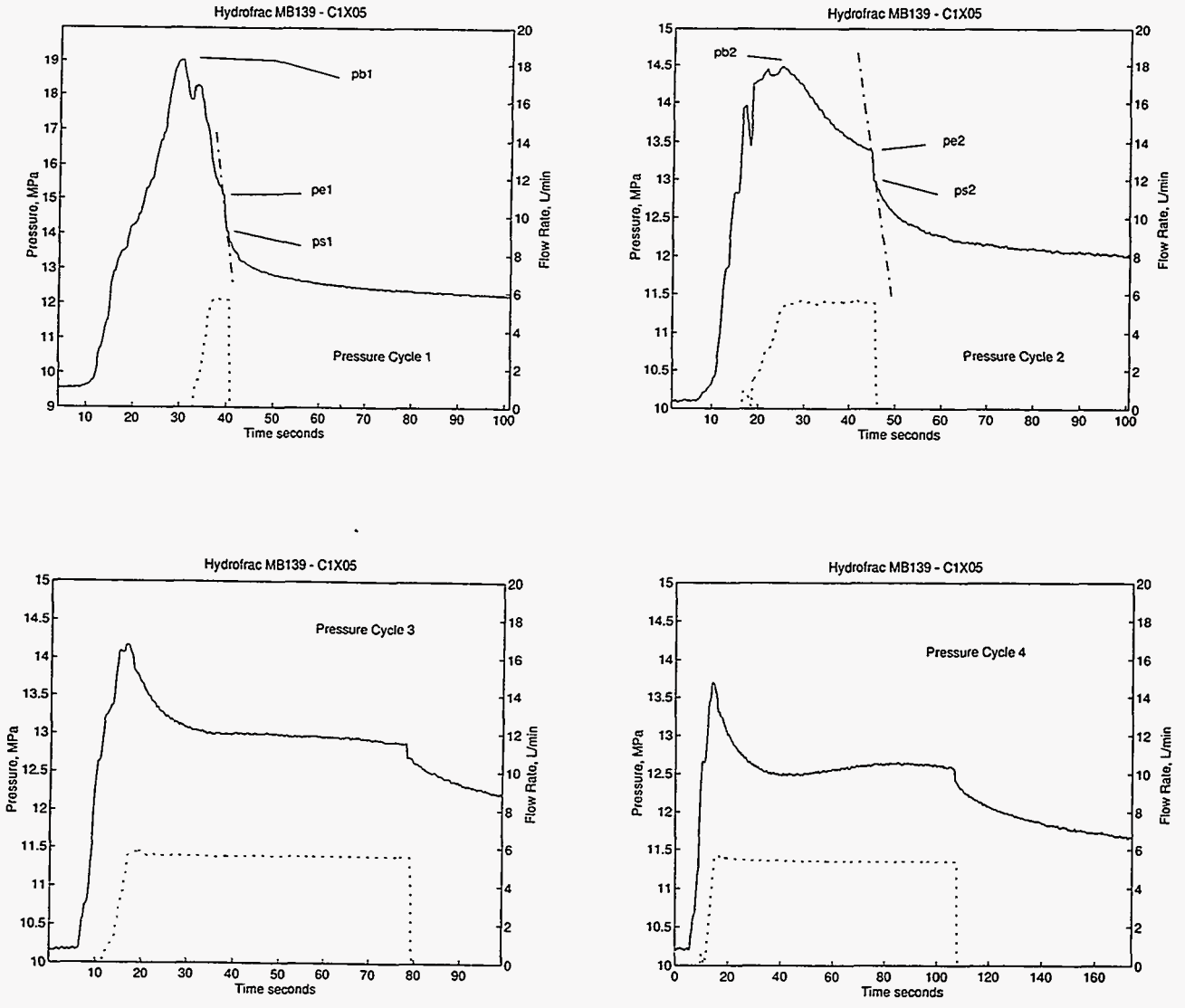

Figure 7 - Pressure-time and flow rate-time records of four-cycle hydraulic fracturing test in MB139, borehole C1X05.

Table 2 - Characteristic pressures of hydraulic fracturing tests in MB139 and MB140. Note: cycle 5 of test in MB140, borehole C1X05, was started approximately 16 hours after cycle 4. Data in square brackets are uncertain because fluid volume injected was not large enough to establish fracture(s) and associated fracture extension pressures.

Marker	Borehole	P_{on} MPa	P_{bn}	P_n	P_n	Flow Rate L/min (Gal/min)	Injection Vol. (L)
MB139	C1X10	7.36	11.63	10.18	9.60	5.7(1.5)	11.6
MB139	C1X05	9.55	19.03	15.13	14.2	5.64(1.49)	>1
		10.09	14.48	13.39	12.90	5.59 (1.47)	2.3
		10.17	14.18	12.89	12.70	5.56 (1.47)	6
		10.21	13.69	12.58	12.37	5.54 (1.46)	9.5
MB140	C1X05	10.54	22.70	[16.4]	16.41	0.24 (?)	>0.5
		10.80	18.50	[15.9]	15.93	4.1 (1.09)	>1
		10.82	18.46	14.8	13.61	5.21 (1.38)	5.8
		11.64	13.24	13.15	≥13.00	0.24 (0.06)	20
		12.10	18.06	14.05	13.36	4.67 (1.23)	8.6
		12.46	15.10	14.14	13.30	4.69 (1.24)	31

Unfortunately, pre-test flow tests did not prevent some sludge from partially clogging a filter between the pump and the flow meter in the first three pressure cycles during hydraulic fracturing in MB140. This problem produced the irregular pressure-time records in pressure cycles 1-3 (Figure 8) and was diagnosed properly only during the third pressure cycle after which the reservoir in the pump was cleaned and the dirty filter replaced. A comparison of the available data, however, suggests that all of the shut-in pressure obtained are valid.

Note that the initial pore pressures in MB139 in boreholes C1X10 and C1X05 differed by at least 2 MPa (290 psi). Such a large pressure differential could only exist if the rock permeability between these two locations was extremely low. The accumulation of at least 15 L (4 gal) of brine and considerable outgassing in C1X10 within 12 hours (overnight) also suggests that borehole C1X10 was placed in or close to a region of relatively high permeability. Because C1X10 was located adjacent to the intersection between Room C1 and the N1420 drift (Figure 2), the local vertical stress after mining probably dropped below the virgin MB139 formation pore pressure. If this happened, the local permeability and storage capacity of MB139 could have been enhanced by mining-induced, pore-pressure-driven hydraulic fracturing. Subsequent brine accumulations in the new, dilated fractures only some 7.6 m (25 ft) below the excavation floor would explain the large amount of brine inflow during 12 hours after borehole C1X10 was completed. In contrast, the brine accumulation in borehole C1X05 near the end of the room in about the same length of time was no more than 50 mL.

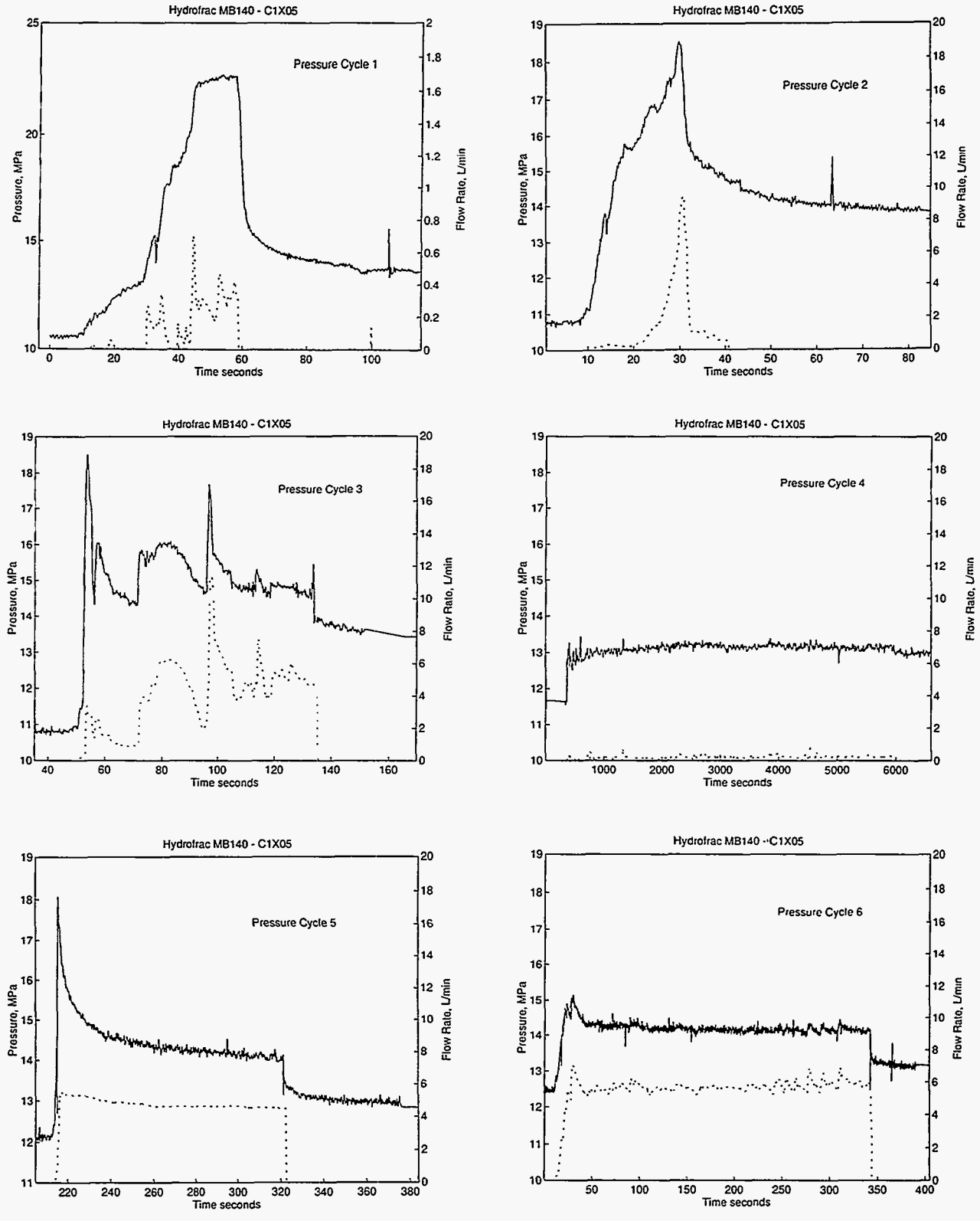

Figure 8 - Pressure-time and flow rate-time records of six-cycle hydraulic fracturing test in MB140, borehole C1X05.

Pressure Response in Hydrologic Observation Boreholes

The existence of the hydrologic observation holes was required to evaluate the permeabilities of MB139 and MB140 during the various stages of testing. However, the presence of these boreholes, including the injection borehole C1X10, also created the unusual opportunity for relating the pressure response at different locations underneath Room C1 to the propagation of the hydraulically driven fractures from C1X05.

As expected, only borehole C1H07 registered the effect of pressure injections into MB139 in C1X05 before the hydraulic fracturing tests. Of course, the observation borehole C1X06 was not drilled until later. The four pressure cycles of the hydraulic fracturing test on day 260 (Table 1) in turn, caused a pressure decline from 8.08 MPa to 7.91 MPa in C1H07 during 4.2 hours after the first injection into C1X05. The pressure drop in C1H07 is interpreted to result from the elastic uplift of the formation as the hydraulically driven fracture advanced. The four-hour pressure decline was followed by an initially rapid and subsequently more gradual, asymptotic pressure increase to 8.38 MPa ten days after hydraulic fracturing.

Noticeable changes occurred when constant-pressure injection experiments were started in borehole C1X05 at 10.4 MPa and 11.62 MPa on test days 322 and 336 (Table 1). Approximately 1 hour after the first injection, the pressure in borehole C1X06 began to decrease until some 15 hours later a hydrologic connection between C1X05 and C1X06 resulted in a sustained pressure rise in C1X06. An equivalent but far more subtle pressure increase, i.e., a weak hydrologic connection, was recorded in C1H07 about 6 days later. When the pressure in C1X05 was stepped up to 11.62 MPa, it appeared that hydraulic fracturing started to advance slowly to the south along the length of room C1. The growth of a crack with time manifested itself in delayed pressure drops followed by gradual elevations in pressure above the local formation pressures in all boreholes as shown in Figure 9. The initial pressure response to the second pressure increase in C1X05 varied from approximately 6 minutes in C1X06 (closest to the injection borehole C1X05) to 40, 88, 130, and 230 minutes in boreholes C1X07, C1H05, C1X10, and C1H06, respectively. Note that C1H06 was drilled under the pillar west of Room C1.

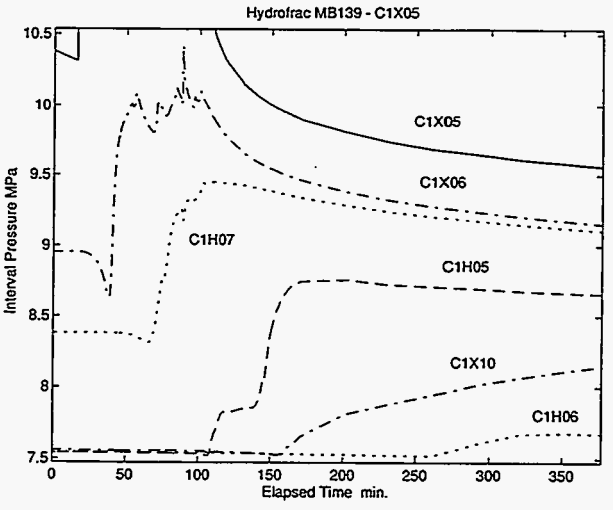

Figure 9 - Pressure-time data demonstrating borehole responses to post-frac pressure injection test in MB139, borehole C1X05. Injection pressure: 11.62 MPa. See Figure 2 for borehole locations.

Pre-frac constant-pressure injection tests in C1X05, MB140 at 10.55-10.71 MPa (1530-1550 psi) for eleven days resulted in only approximately 3 mL of fluid injection. Because of the

small volume of fluid involved, no pressure response was observed in the adjacent observation boreholes. At the same time, the associated small pressure change (0.2 MPa; Table 1) in the lower interval of C1X05 demonstrated that interactions between the upper and lower intervals were limited to the transmission of pressure pulses through the middle packer element of the straddle packer.

Hydraulic fracturing attempts during the first two pressure cycles in MB140 involved less than 1 L of fluid injection per cycle. The lack of a pressure response in the nearby observation hole C1X06 (Figure 2) suggests that these small quantities of fluid had initiated a hydraulic fracture that was small compared with the 3-m distance between the injection borehole C1X05 and C1X06. A quick connection was established only during the third pressure cycle associated with 5.8 L of fluid flow (Table 2). It was surprising at first that the new flow path appeared to link the upper interval of the injector C1X05 with the lower interval in borehole C1X06. Inspections of the test records at a later time, however, indicated that the packer elements in C1X06 had been placed slightly but sufficiently higher to make it possible that a fracture starting near the bottom of the upper interval in C1X05 could intersect the very upper part of the lower interval in borehole C1X06 (Appendix A). The pressure in the latter two intervals became equal during the fourth hydraulic fracturing cycle indicating a complete connection.

Fracture growth during the fourth pressure cycle and 20 L of fluid injection appeared to be reflected in a small pressure drop in the lower interval in borehole C1H07. After the six-cycle hydraulic fracturing tests (Figure 8) had been completed, the pressures in the upper and lower intervals of the injector hole C1X05 equalized around 11.7 MPa. In turn, the upper and lower intervals of the two observations boreholes C1X06 and C1H07 appeared to remain isolated and at different pressures consistent with the distinctly different initial, pre-hydrofrac formation pressures in these two zones. Responses observed in the upper and lower intervals of boreholes C1X05 and C1X06 to later pressure fluctuations in C1H07 caused by tool problems confirmed that the main connections were between the lower intervals of C1X06 and C1H07 and the upper interval of C1X05.

Post-Test Visual Fracture Observations

Post-hydraulic fracture observations relied almost exclusively on borehole video surveys using either white light, or in the majority of cases, ultraviolet illumination suitable for distinguishing natural brine from hydraulic fracturing fluid with fluorescent dye. The borehole inspections included (1) all of the holes drilled prior to or during the experiments for monitoring of formation pressure and fluid flow (Figure 2), and (2) the boreholes that were put down after the completion of testing (Figure 3), beginning in November 1994. In general, if present, the dye signatures were very distinct in new boreholes that had not been drained repeatedly and over extended periods of time. Unfortunately, the dye traces were spottiest and ambiguous in the main injection borehole C1X05 both in MB139 and MB140. It must be assumed that parts of the hydraulically induced fractures intersected areas with large natural brine accumulations that were then allowed to flow towards the injection hole. When this happened, the uncolored brine probably washed away the residual fluorescent dye that is needed in order to identify the character of the hydraulic fractures.

As expected, dye was found in both Marker Beds in the active test holes (C1X05, C1X06, C1H07, C1X10, C1H05, and C1H06, Figure 2), as well as in the new observation borehole C1X12 that lies close to a connecting line between C1X05 and C1H07 (Figure 3a). A well-defined, inclined fracture with fluorescent dye was also seen in borehole C1X07 (Figure 3a) at the upper contact of MB139. Other fracture traces were noted in borehole C1X11 in MB140 approximately 4.5 m east of the eastern boundary of Room C1, i.e., under the pillar east of C1. On the other hand, absolutely no evidence of hydraulically induced fractures was found in MB139, boreholes C1X08 and C1X11, and in MB140, boreholes C1X07 and C1X08 (Figure 3a). An oily smell was noted during handling of core from MB139, C1X09, but this smell did not correlate with dye traces in the corresponding video tape.

Four video records are shown in Figure 10 indicating the dye traces that appeared to be most typical. Depth correlations of these records with core photographs revealed that hydraulic fracturing occurred in the interbed Zones II, III, and IV as defined by Borns (1985; Appendix B and Figure 4). Almost all of the continuous fracture traces were subhorizontal as shown in Figure 10a-10c. Several locations exhibited up to four fracture branches spaced 0.5 cm (0.2 in) to 2 cm (0.8 in) apart each. In boreholes C1X06 and C1X12, for example, a set of such subhorizontal fractures appeared to lie in an approximately 10 cm (4 in) high band reminiscent of the network of partially or fully infilled fractures in the Zones II and IV in Figures 5a and 5b. In every borehole, however, one main fracture stood out because it still produced dyed fluid as well as gas. These dominant fractures always appeared to be located in Zones III or IV. Unmistakable Zone-II fractures were recognized in the video tapes of borehole C1X05 where distinct fluid/gas bubbles emanated primarily from the upper contact of partially healed fractures (Figure 5a). In some instances, the main fractures were sharply delineated; in others, they give way to patches with smaller fractures each of which actively produced dyed fluid and gas. It was also typical that even well-defined fractures did not produce fluid uniformly but rather exhibited evidence of channel flow.

Although subhorizontal fracturing was typical, nearly all video records exhibited some short, jagged subvertical fractures. The example in Figure 10d was taped in borehole C1X06. It looked as if the subvertical fracture traces shown eventually terminated at two subhorizontal fractures several centimeters apart.

Observational work is continuing to determine how hydraulic fracturing was initiated in borehole C1X05. Analyses by Roegiers (1974) and Warren (1981) showed that tensile stresses in a packed-off borehole parallel to the borehole axis and close to the packers become significant as the difference between the packer pressure and the interval pressure increases. Because this difference reached several MPa during the first pressure cycles of the hydraulic fracturing tests in C1X05, it is possible that a combination of vertical tension, tensile strength anisotropy, and the presence of partially open (or only partially infilled) subhorizontal stress risers could have resulted in horizontal fracture initiation. Under normal circumstances and in isotropic rocks it would be more likely that failure started as vertical fractures that turned direction to propagate horizontally, perpendicular to what would have to be the minimum in situ principal stress under Room C1.

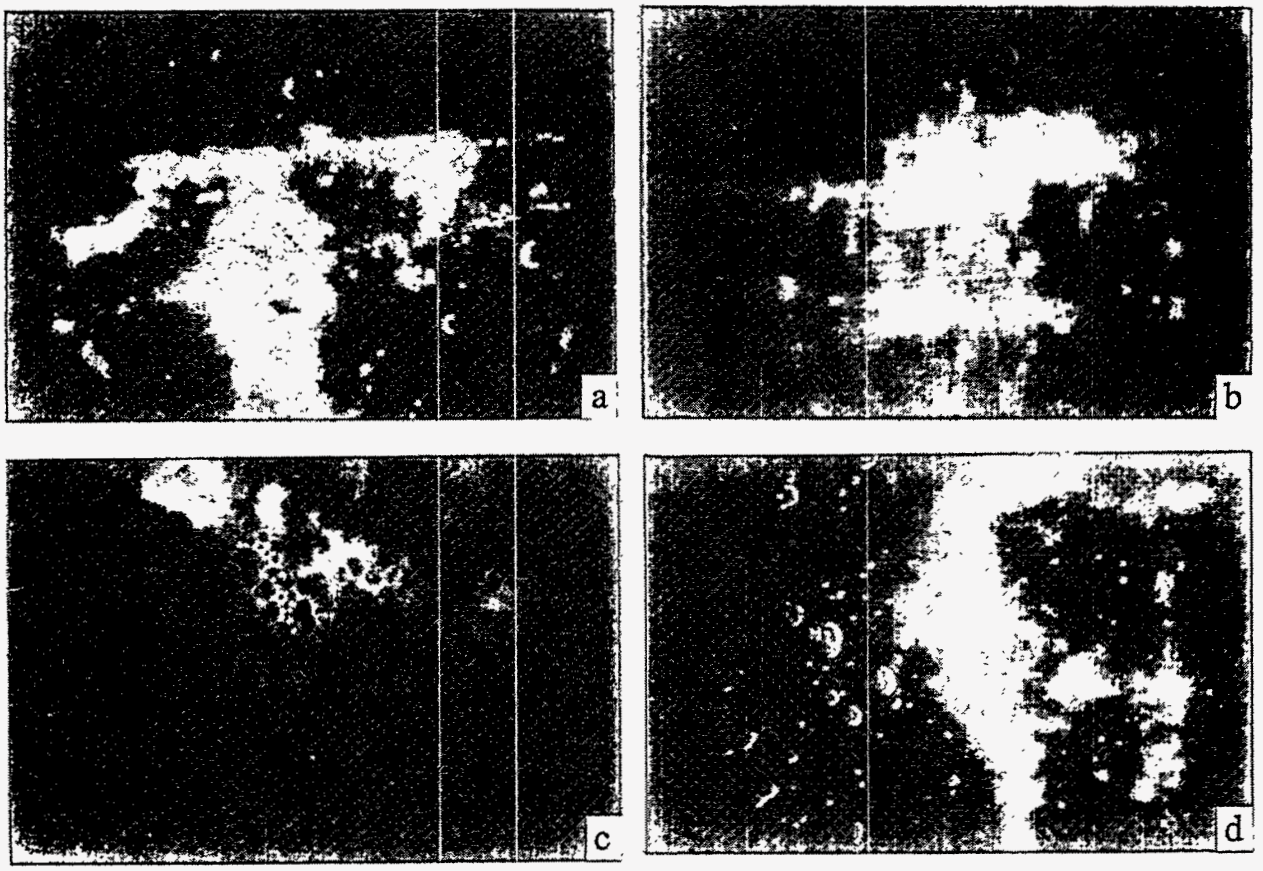

Figure 10 - Borehole video records showing fluorescent dye and fluid/gas bubbles associated with hydraulic fractures. (a) Borehole C1X06, MB140 with two well-defined subhorizontal fracture traces, (b) borehole C1X12, MB140 exhibiting two of a set of multiple subhorizontal fractures, (c) borehole C1X12, MB139 with pronounced local (channel) flow along a distinct subhorizontal fracture, and (d) borehole C1X06, MB140 with trace of a subvertical fracture. Note: height of images is 1.1 cm (0.44 in).

10. Discussion

The hydraulic fracturing tests in this study were integrated with in situ flow measurements to determine the influence of discrete fractures on the permeability of MB139 and possibly other interbeds above and below the repository horizon in the WIPP. By themselves, the hydraulic fracturing measurements were meant to address six issues: (1) At what fluid pressures will fracturing occur in MB139 and MB140 both in potentially disturbed and undisturbed (virgin) states? (2) If fracture took place, would it take place and be contained along preexisting weakness planes or not? (3) What pressures would be required to propagate any liquid- or gas-driven fractures, and also, (4) What could be said about the path of new fractures within or potentially out of the Marker Bed? Clearly, the last issue is directly related to: (5) is the virgin stress state in MB139 isotropic as in the surrounding rock salt, and if not, (6) what is the magnitude and direction of the least compressive in situ principal stress?

The comparison of instantaneous shut-in pressures in MB139 (9.6 and 12.37 MPa; 1390 and 1790 psi MB139; Table 2) with the virgin in situ stress at the WIPP horizon (14.9 MPa; Wawersik and Stone, 1989) indicates that the virgin stress field in MB139 was altered due to the presence of existing WIPP excavations. This result was not totally surprising in the light of numerical predictions of stresses in the floor salt of Room C1 (Argüello, 1991). It was unexpected, however, that the variations in the stress states in MB139 as well as MB140 were large enough to essentially limit the advance of the hydraulic fractures from the injection borehole C1X05 at the northern end of Room C1 to the region below and parallel to the room floor where the local stresses, especially the local overburden stresses had been reduced. Because no hydraulic fracture measurements were made in virgin ground, the results of the present study are less general than anticipated.

At this time it is unclear whether hydraulic fracturing was initiated by horizontal fracturing at all three test stations. Based on multiple borehole observations, however, it is clear that the overall hydraulic fracture orientations were horizontal. Therefore, it follows that hydraulic fracture propagation was dominated by the local vertical stresses in both marker beds probably aided by strength anisotropies due to preexisting horizontal weakness planes. It also follows hat the local principal horizontal stresses in the interbeds were not significantly smaller than the local vertical stresses that are indicated by the instantaneous shut-in pressures of 13.3 MPa (1930 psi) or less (Table 2).

Argüello (1991) calculated that the vertical stresses 7.6 m (25 ft) below Room C1 should be 9.83 MPa at the location of borehole C1X10 and 13 MPa at C1X05 (Fig. 2). Because hydraulic fracturing from borehole C1X05 propagated under Room C1, these stresses should establish the lower bound pressures needed to maintain hydraulic fracture growth. Accordingly, the fracture extension pressures in MB139 under C1 should be 13 MPa near C1X05 and decreasing with fracture advance to the south towards C1X10. This is precisely what happened. The lowest fracture extension pressure during the fourth and last pressure cycle in borehole C1X05 was 12.58 MPa. It is noted that the apparent differences between calculated local vertical stresses and the fracture extension pressures are quite small, suggesting that horizontal fracture propagation distant from the WIPP will take place at pressures that are only slightly larger than the overburden stress of around 15 MPa. The small difference between fracture opening and fracture extension pressure is unambiguously demonstrated by the fact that the fracture extension pressure and the instantaneous shut-in pressure were nearly equal at the very slow flow rate of 0.24 L/min (0.06 gpm) during the fourth pressure cycle in borehole C1X05, MB140 (Table 2).

The pronounced difference in pre-frac formation permeabilities and initial hydraulic fracturing breakdown pressures between C1X05 and C1X10 point to a considerable variation in rock disturbance close to the entry and near the end of Room C1. A low pre-frac permeability in borehole C1X05 (Fig. 2), MB139 (10^{-20} m^2) suggests that the stress changes associated with mining of Room C1 left the interbed rock essentially intact near the end of C1. On the other hand, major effects of mining around borehole C1X10 (Fig. 2) resulted in an order-of-magnitude increase in permeability. In the former case, the initial breakdown pressure during hydraulic fracturing constitutes an upper bound for the initiation of a fluid-induced interbed fracture. This upper bound estimate lies between 19 MPa (2720 psi, primary breakdown pressure in MB139)

and 22.5 MPa (3260 psi, primary breakdown pressure in MB140; Table 2). Decreasing rates of borehole pressurization would have resulted in reductions in primary breakdown pressures because of time- or rate-dependent material weakening (Atkinson, 1987) and fluid diffusion into the pore spaces (Haimson and Fairhurst, 1967).

Observations concerning the geometry of the hydraulically induced fractures in borehole C1X05, MB139 and MB140 strongly suggest that the shape of pressure-driven fractures is locally sensitive to relatively small variations in the in situ stresses. Apparently, the differences in the vertical stresses in and immediately adjacent to the vertical projections of Room C1 onto the marker beds were large enough to constrain hydraulic fracture development to an approximately rectangular area not only in MB139 but even in the 25-m deeper MB140 This follows from the visual borehole fracture observations and from the linear delay in the pressure response in boreholes C1X06, C1H07, C1H05, and C1X10 in MB139 with distance from the injection borehole C1X05 (Figures 2 and 9). Radial fracture propagation at a constant injection rate should yield an approximately square-root dependence of delay time. The only MB139 fracture falling outside the vertical projection of Room C1 onto the top of MB139 was observed in borehole C1X07 merely 2.5 m (8 ft) north of the injection hole C1X05. Termination of this fracture at the upper contact of MB139 and its dip of some 45° to the south substantiate the stress-sensitivity of hydraulic fracturing paths.

Preferred hydraulic fracturing in MB139 Zones II, III, and IV suggests that the stress-sensitivity of hydraulic fracture propagation is enhanced by lithological and structural heterogeneity of the formation. The same appears to hold for fracture aperture and fracture permeability at the present test location and most likely also distant from the existing WIPP openings. In particular, newly formed fractures are not always discrete but rather may advance by opening networks of subparallel, partially healed preexisting fractures in the top and bottom thirds of MB139, Zones II and IV according to Borns (1985). It is also apparent that fluid flow through fractures after shut-in, i.e., after newly formed fractures are allowed to come back into contact, occurs along many channels and not uniformly as between smooth parallel plates. Published descriptions of such flow conditions (Brown, 1987) demonstrate that the conductivity of rough fractures, and therefore, the average permeability of a fractured MB139 will change dramatically with aperture. The aperture, in turn, is determined by the magnitude of the fluid pressure within the fracture and by the magnitude of the stress normal to the fracture (Beauheim et al., 1993b; Brown, 1987).

Credible estimates can be made of the absolute and relative magnitudes of the horizontal principal stresses at the test locations in MB140 and beyond. The presence of some short but distinct subvertical fractures (Figure 10d) in conjunction with fully developed and pervasive horizontal fractures points to a relatively small, but only a small, difference between the local vertical and minimum horizontal principal stresses. This also implies that the maximum and minimum horizontal stresses are essentially equal. The same conclusion is indicated by customary estimates of the total horizontal in situ stresses in bedded rock. Assuming poroelastic conditions (Engelder, 1993), plane-strain deformation, a far-field overburden stress $\sigma_v \approx 15.2$ MPa (2200 psi), an initial pore pressure p_{o1}=10.54 MPa (Table 2), and a Poisson's υ=0.35 for anhydrite (Teufel, 1981),

$$\sigma_H \approx \sigma_h = (\frac{\upsilon}{1-\upsilon})\sigma_v + \alpha p_{ol}(1-\frac{\upsilon}{1-\upsilon}) = 13 \text{ MPa},$$

where σ_H and σ_h are the greatest and smallest horizontal principal stresses and $\alpha \leq 1$. It is almost certain that the presence of Room C1 produced a reduction in pore pressure as WIPP rooms were excavated only some 25 m above. Therefore, using pore pressures $p_o \geq 12.5$ MPa that were measured in MB139 under pillars and 23 m (75 ft) horizontally beyond any existing WIPP openings (Beauheim et al., 1993a; Domski et al., 1996), yields $\sigma_H \approx \sigma_h = 13.95$ MPa. This results in a smaller principal stress difference and associated ratio (σ_v/σ_H). Some difference between the vertical and horizontal principal stresses in anhydrite is plausible because the yield stress of anhydrite equals or exceeds 90 MPa (Teufel, 1981), and because the creep resistance of anhydrite far exceeds that of rock salt (Mueller and Briegel, 1978).

A substantially different but less believable result is obtained if the high and consistent breakdown pressures during the second and third pressure cycle in C1X05, MB140 (Table 2) are attributed to the formation of a vertical fracture at the borehole wall. If the borehole stresses under this condition were elastic, then the subsequent breakdown (or reopening) pressures around the borehole become

$$p_{bn}=3\sigma_h - \sigma_H = 3\sigma_h (1-n)$$

where n denotes the ratio $n=(\sigma_H/\sigma_h) \geq 1$. Using $p_{bn}=18.5$ MPa (2680 psi; Table 2), $9.25 \leq \sigma_h \leq 10.28$ MPa (1340-1490 psi) for $1 \leq n \leq 1.2$. It is inconceivable that hydraulic fracturing under such stress conditions would have led to the development of horizontal fractures. On the other hand, if the rock at the borehole location had undergone some plastic deformation, then the elastic hoop stresses would have relaxed and $\sigma_H \approx \sigma_h$ would be predicted to increase and approach the value of the measured local vertical principal stress of 13 MPa (1890 psi). This argument returns the reasoning to its starting point.

Extrapolations of the local in situ stress determinations are possible on the basis of the structural mechanics calculations of Argüello (1991). Based on Argüello's analyses, mining of Room C1 produces significantly smaller reductions in the horizontal than in the vertical in situ stresses. It is suggested, therefore, that the horizontal stress magnitudes inferred above, $\sigma_H \approx \sigma_h \approx$ 13 MPa (1890 psi), are indeed representative of the horizontal in situ stresses distant from the WIPP and that the vertical stress everywhere is equal to the integrated overburden density as was verified in rock salt in the G-drift (Wawersik and Stone, 1989).

Because the present tests involved short, no more than approximately 30-m long fractures in more or less stress-altered zones around the WIPP, our experiments do not resolve whether or not gas pressure will initiate horizontal fractures at marker- bed locations remote from the WIPP and whether and how far from the WIPP fluid-driven, especially gas-driven, fractures will remain horizontal and confined to MB139 or any other marker bed. Given the estimated difference between virgin vertical and horizontal principal stresses ($\sigma_v - \sigma_h \approx 2$ MPa/290 psi), it is conceivable that horizontal hydraulic fractures might become vertical (Haimson, 1974) if the

marker beds consisted of homogeneous, isotropic rocks. Because of the pronounced lithological and structural anisotropies of MB139 and MB140, however, we believe (but cannot prove) that vertical fracturing will require a higher contrast between vertical and horizontal in situ stresses.

Ongoing axisymmetric approximations deal with the consequences of fracture length. Assuming that locally discrete or up to several cm thick zones of anastomosing fractures all can be described by a dominant discrete fracture, linear elastic fracture mechanics calculations (Gerstle et al., 1996) indicate that a pressurized crack could curve upwards out of an interbed as the ratio of crack length to crack depth below surface increases. Upward fracture growth is more likely if the applicable fracture toughness for anhydrite becomes greater than approximately 0.6 times the fracture toughness for rock salt. This independent result by Gerstle et al. (1996) agrees with an earlier plane-strain analytical solution by Pollard and Holzhausen (1979) concerning the behavior of an arbitrarily oriented pressurized crack in the vicinity of a free surface. In either case, the theoretical possibility of fracture growth out of an interbed will depend primarily on the length of the fractures that are required to accommodate the amount of gas that is generated in the WIPP. However, it is emphasized that neither Gerstle's or Pollard and Holzhausen's calculations consider the potentially overriding influence of rock anisotropy. We believe that the upward growth of horizontal fractures out of the interbeds, especially MB139, becomes unlikely if the preexisting weakness planes in MB139 act as regionally pervasive fracture guides. These weakness planes are typical throughout the WIPP excavations.

We reported previously (Beauheim et al., 1993b) that 67% of all fluid injected into MB139 through borehole C1X05 was recovered. This implied that about 6 L of fracturing fluid were left to suggest a residual fracture aperture of approximately 0.2 mm (0.008 in). The corresponding average fracture opening during the last and most extensive pressure cycle in MB139 was approximately 0.3 mm (0.012 in). The presence of the fracture and the influence of pressure on fracture opening (aperture), explain the orders-of-magnitude differences between the formation permeabilities before and after the hydraulic fracturing tests in MB139 (Beauheim et al., 1993b). Ongoing data analyses will determine the degree of correspondence between the events in MB139 and MB140. The observed frac-fluid recoveries were 75% during the first four pump cycles that included the slow-rate, 20-L (5.3 gal) pump (Table 2). However, only about 57% of the frac fluid was recovered after the last, 31-L injection, and it was surprising that the three-times larger amount of fluid injection into MB140 compared with MB139 did not produce any recognizable fracture traces in every observation hole, especially C1X13 (Figure 3). It is possible that the overall reach of the hydraulically induced fracture in MB140 was reduced by the development of numerous branch fractures as indicated by some post-fracturing borehole observations described earlier. If the footprints of the hydraulic fractures in MB139 and MB140 were the same, then a fluid loss of some 13 L (3.4 gal) and the formation of more branch fractures in MB140 would yield an effective residual fracture opening of over 0.4 mm (0.016 in).

11. Summary and Conclusions

Hydraulic fracturing tests were integrated with hydrologic tests to estimate the conditions under which gas pressure in the disposal rooms in the WIPP will initiate and advance fracturing in nearby interbeds, especially MB139. The measurements were made in MB139 and MB140 in the

north-east part of the WIPP experimental area. The particular location in Room C1 was selected because of the possibility that MB139 might not be disturbed much by existing mine openings and that the approximately 17-m deeper MB140 might lie completely outside the field of influence of the WIPP. Post-test fracture observations revealed that these expectations were not met, and therefore the results of this study are less general than anticipated.

Hydraulic fracturing experiments were carried out rapidly and with a thin hydraulic oil rather than gas in order to obtain upper-bound estimates of the pressures needed to initiate and to propagate hydraulically induced fractures. Upper-bound pressures were of interest to determine the greatest possible gas pressure in the disposal rooms. Fluorescent dye in the fracturing fluid and nearby observations holes were used to identify the orientation and shape of the hydraulic fractures, whether these fractures consisted of single or multiple branches, and whether they were influenced by preexisting partially healed natural fractures, i.e., preexisting weakness planes.

The following major results and conclusions were obtained:

(1) The upper part of MB140 is a valid analog of MB139 for studying interbed fracture at greater distances from present WIPP excavations than are accessible in MB139. However, the hydraulic fracturing locations in both interbeds were not yet in undisturbed ground.

(2) The maximum breakdown pressures and the pressures necessary to sustain fracture propagation ranged from approximately 19 and 12 MPa (2760, 1740 psi) in MB139 to 22 and 13 MPa (3190, 1890 psi) in the deeper MB140, respectively. The fracture initiation pressure can drop by several MPa at the location of preexisting, open fluid-filled and pressurized fractures. This happened in the trial test hole C1X10 at a primary breakdown pressure, p_{b1}=11.6 MPa (1686 psi).

(3) The smallest principal compressive stresses at both test locations were vertical resulting in predominantly horizontal hydraulic fracture development aided by strength anisotropies due to preexisting horizontal weakness planes.

(4) Hydraulically induced fractures exhibited dominant fractures but also developed anastomosing branches along networks of subparallel, partially healed preexisting fractures or weakness planes in the top and bottom thirds of MB139 and analogous lithologies in MB140. The existence of branch fractures may provide fluid storage capacity over the storage capacity of discrete fractures. However, their presence is not believed to invalidate the applicability of linear elastic fracture mechanics to estimate the pressures that are needed to advance the dominant fractures.

(5) Clear instantaneous shut-in pressures yielded the magnitudes of the least local principal (vertical) compressive stresses: 12.4 MPa (1800 psi) in MB139 and 13.3 (1930 psi) in MB140. Both values are less than the overburden stress calculated from integrated overburden densities and confirmed by hydraulic fracturing stress measurements in WIPP salt. Both values agree with stresses that were determined in separate finite element calculations.

(6) The induced fracture patterns and, especially, the formation of some subvertical fractures indicate that the horizontal principal stresses in MB140 are equal or nearly equal to the measured local vertical stress. Separately, poroelastic estimates suggest that the virgin horizontal principal stresses in MB139 and MB140 are approximately equal or greater than 13 MPa (1890 psi), i.e., up to 2 MPa (290 psi) lower than the overburden stress. Based on finite element results, the range of these horizontal principal stress values is deemed representative of the principal horizontal stresses in virgin ground.

(7) The hydraulic fracturing tests completed in MB139 and MB140 demonstrate that hydraulically induced fractures in MB139 and MB140 can propagate horizontally within the interbeds. However, the tests do not prove that horizontal fracture growth will persist in undisturbed rock distant from the WIPP. Published and ongoing linear elastic fracture mechanics analyses indicate that fractures may leave the interbeds as they become long compared with the depth below surface even if the stress states in the marker beds were perfectly isotropic. For isotropic rock properties, it is also conceivable that a far-field stress difference of $(\sigma_v - \sigma_h) \approx 2$ MPa (290 psi) could be large enough to result in fracture reorientation from horizontal to vertical. Both upward growth of horizontal fractures out of the interbeds, especially MB139, and a change of fracture orientation from horizontal to vertical are unlikely if the preexisting weakness planes in MB139 (typical under the existing WIPP excavations) continued to act as regionally pervasive fracture guides. Vertical fracture growth is highly unlikely if separate pore-pressure measurements in relatively undisturbed portions of MB139 are representative of the interbed pore pressures in the far field.

(8) The creation of pressure-driven fractures and residual fracture openings of 0.2 to approximately 0.4 mm after hydraulic fracturing explain orders-of-magnitude changes in interbed permeabilities before and after hydraulic fracturing and a strong dependence of post-frac interbed permeability on pressure.

12. References.

Argüello, J.G. 1991. *Pretest 3-D Finite Element Analysis of the WIPP Intermediate Scale Borehole Test.* SAND90-2055. Albuquerque, NM: Sandia National Laboratories.

Atkinson, B.K. 1987. "The Theory of Subcritical Crack Growth with Application for Minerals and Rocks," *Fracture Mechanics of Rocks.* Ed. B.K. Atkinson. New York, NY: Academic Press. 111-166.

Beauheim, R.L., G.J. Saulnier, Jr., and J.D. Avis. 1991. *Interpretation of Brine-Permeability Tests of the Salado Formation at the Waste Isolation Pilot Plant Site: First Interim Report.* SAND90-0083. Albuquerque, NM: Sandia National Laboratories.

Beauheim, R.L., R.M. Roberts, T.F. Dale, M.D. Fort, and W.A. Stensrud. 1993a. *Hydraulic Testing of Salado Formation Evaporites at the Waste Isolation Pilot Plant Site: Second Interpretive Report.* SAND92-0533. Albuquerque, NM: Sandia National Laboratories.

Beauheim, R.L., W.R. Wawersik, and R.M. Roberts. 1993b. "Coupled Permeability and Hydrofracture Tests to Assess the Waste-Containment Properties of Fractured Anhydrite," *International Journal of Rock Mechanics and Mining Sciences & Geomechanics Abstracts*. Vol. 30, no. 7, 1159-1163.

Borns, D.J. 1985. *Marker Bed 139: A Study of Drillcore From A Systematic Array.* SAND85-0023. Albuquerque, NM: Sandia National Laboratories.

Brown, S.R. 1987. "Fluid Flow Through Rock Joints: The Effect of Surface Roughness," *Journal of Geophysical Research*. Vol. 92, no. B2, 1337-1347.

Davies, P.B. 1991. *Evaluation of the Role of Threshold Pressure in Controlling Flow of Waste-Generated Gas into Bedded Salt at the Waste Isolation Pilot Plant.* SAND90-3246. Albuquerque, NM: Sandia National Laboratories.

Davies, P.B., G. Freeze, M. Reeves, and T. Cauffman. 1990. "Status Report on Multi-Phase Simulations of Waste-Generated Gas at the WIPP Repository." Viewgraph Presentation to NAS WIPP Review Panel. Washington, D.C. Albuquerque, NM: Sandia National Laboratories. (Copy on file at the Sandia WIPP Central Files, Sandia National Laboratories, Albuquerque, NM as WP08703.)

Domski, P.S., D.T. Upton, and R.L. Beauheim. 1996. *Hydraulic Testing Around Room Q: Evaluation of the Effects of Mining on the Hydraulic Properties of Salado Evaporites.* SAND96-0435. Albuquerque, NM: Sandia National Laboratories.

Engelder, T. 1993. *Stress Regimes in the Lithosphere*. Princeton, NJ: Princeton University Press.

Gerstle, W., M. Xie, Q. Liu, and Z. Chen. 1996. "Gas-Driven Cracking in WIPP Rock Salt," *Radioactive Waste Management and Environmental Restoration*. Vol. 20, nos. 2-3, 93-110.

Haimson, B.C. 1974. *Determination of In-Situ Stresses Around Underground Excavations by Means of Hydraulic Fracturing*. Final Tech. Rep. Contract No. H0220080. Madison, WI: Engineering Experiment Station, University of Wisconsin. (Available from National Technical Information Service (NTIS), Springfield, VA. Telephone: 703/487-4650. NTIS Order Number: AD-780 220/0.)

Haimson, B.C., and C. Fairhurst. 1967. "Initiation and Extension of Hydraulic Fractures in Rocks," *Society of Petroleum Engineers Journal*. Vol. 7, no. 3, 310-318.

Holt, R.M., and D.W. Powers. 1984. *Geotechnical Activities in the Waste Handling Shaft, Waste Isolation Pilot Plant (WIPP) Project, Southeastern New Mexico.* WTSD-TME-038. Carlsbad, NM: U.S. Department of Energy, Waste Isolation Pilot Plant.

Krieg, R.D. 1984. *Reference Stratigraphy and Rock Properties for the Waste Isolation Pilot Plant (WIPP) Project.* SAND83-1908. Albuquerque, NM: Sandia National Laboratories.

Mueller, W.H., and U. Briegel. 1978. "The Rheological Behaviour of Polycrystalline Anhydrite," *Eclogae Geologicae Helvetiae.* Vol. 71, no. 2, 397-407.

Pollard, D.D., and G. Holzhausen. 1979. "On the Mechanical Interaction Between a Fluid-Filled Fracture and the Earth's Surface," *Tectonophysics.* Vol. 53, 27-59.

Roegiers, J.C. 1974. "The Development and Evaluation of a Field Method for In Situ Stress Determination Using Hydraulic Fracturing." Ph.D. dissertation. Minneapolis, MN: University of Minnesota.

Stormont, J.C., E.W. Peterson, and P.L. Lagus. 1987. *Summary of and Observations About WIPP Facility Horizon Flow Measurements Through 1986.* SAND87-0176. Albuquerque, NM: Sandia National Laboratories.

Stormont, J.C. 1990a. *Summary of 1988 WIPP Facility Horizon Gas Flow Measurements.* SAND89-2497. Albuquerque, NM: Sandia National Laboratories.

Stormont, J.C. 1990b. *Discontinuous Behavior Near Excavations in a Bedded Salt Formation.* SAND89-2403. Albuquerque, NM: Sandia National Laboratories.

Stormont, J.C., C.L. Howard, and J.J.K. Daemen. 1991. *In Situ Measurements of Rock Salt Permeability Changes Due to Nearby Excavation.* SAND90-3134. Albuquerque, NM: Sandia National Laboratories.

Teufel, L.W. 1981. *Mechanical Properties of Anhydrite and Polyhalite in Quasi-Static Triaxial Compression.* SAND81-0858. Albuquerque, NM: Sandia National Laboratories.

Warren, W.E. 1981. "Packer-Induced Stresses During Hydraulic Well Fracturing," *Journal of Energy Resources Technology, Transactions of the ASME.* Vol. 103, no. 4, 336-343.

Wawersik, W.R. 1991-1993. "Activity-Specific ES&H Standard Operating Procedure Instructions for Hydraulic Fracturing Tests in MB139 and MB140." SP471962, Issues A-C. Albuquerque, NM: Sandia National Laboratories. (Copy on file in the Sandia WIPP Central Files, Sandia National Laboratories, Albuquerque, NM, as WPO38248, WPO38249, and WPO 38251.)

Wawersik, W.R., and R.L. Beauheim. 1991. *Test Plan - Hydraulic Fracturing and Hydrologic Tests in Marker Beds 139 and 140.* DOE/DP/00789-T271. Albuquerque, NM: Sandia National Laboratories.

Wawersik, W.R., and C.M. Stone. 1985. *Application of Hydraulic Fracturing to Determine Virgin In Situ Stress State Around Waste Isolation Pilot Plant - In Situ Measurements.* SAND85-1776. Albuquerque, NM: Sandia National Laboratories.

Wawersik, W.R. and C.M. Stone. 1989. "A Characterization of Pressure Records in Inelastic Rock Demonstrated by Hydraulic Fracturing Measurements in Salt," *International Journal of Rock Mechanics and Mining Sciences & Geomechanics Abstracts.* Vol. 26, no. 6, 613-627.

This page intentionally left blank.

Appendix A -Depths of Interbed Boundaries and Hydraulic Fracturing Intervals

Borehole ID	MB No.	MB Location*		Interval Location m(ft)		Clay Seam Centers m(ft)
		Top	Bottom	Top	Bottom	
C1X05	140	23.08 (75.5)	27.14 (89.0)	23.48 (77.0) 25.58 (83.9)	24.82 (81.4) 27.87 (91.4)	26.34 (86.4) and 27.13 (89.0)
C1X06	140	22.96 (75.3)	27.13 (89.0)	22.68 (74.4) 24.27 (79.6)	23.66 (77.6) 27.35 (89.7)	26.27 (86.2) and 27.05 (88.7)
C1H07	140	22.8 (74.8)	27.23 (89.3)	22.97 (75.3) 24.56 (80.56)	23.95 (78.6) 27.88 (91.45)	26.55 (87.1) and 27.20 (89.2)
C1X10	139	7.51 (24.6)	8.26 (27.1)	7.54 (20.3)	8.22 (27.0)	
C1H05	139	7.13 (23.4)	7.90 (25.9)	7.00 (23.0)	8.22 (27.0)	
C1H06	139	7.49 (24.6)	8.08 (26.5)	7.30 (23.9)	8.38 (27.5)	
C1X05	139	6.65 (21.8)	7.60 (24.9)	6.72 (22.1)	7.50 (24.6)	
C1X06	139	6.43 (21.1)	7.32 (24.0)	5.87 (19.3)	7.63 (25.0)	
C1H07	139	6.77 (22.2)	7.70 (24.7)	6.44 (21.1)	8.17 (26.8)	

*Note: All depths are referenced to the collar locations of the boreholes shown. The depths of the top and bottom of MB139 and MB140 listed were taken from field notebooks that were maintained by the experiment staff of the two Sandia organizations involved, the Geohydrology Department and the Geomechanics Department. Small discrepancies in depth determinations were noted in subsequent comparisons between the field notes and the descriptions of core photographs as indicated in Appendix B. These discrepancies are attributed to occasional difficulties in identifying and therefore including the thin uppermost Zone I.

Appendix B -Core descriptions, MB139 and MB140

NOTE: The depths of the top and bottom of MB139 and MB140 listed in the headers and in the entries of the following tables were established at different times, by different individuals, and under different circumstances, i.e., under poor lighting conditions, underground versus office lighting conditions. The header data were taken from the field notebooks that were maintained by the experiment staff of the two Sandia organizations involved, the Geohydrology Department and the Geomechanics Department. The row entries were read off core photographs at a later time. Some discrepancies in the two data sets are attributed to difficulties in identifying clay-rich zones such as Zone I (Figure 4).

WIPP Core Description Room C1, Borehole C1X05
Marker Bed 139
Depth of top/bottom contacts, m/ft: 6.65-7.60m / 21.8-24.9'
Date: June 10, 1994

Interval m.	Marker Bed Zone from Borns (1985)	Description:	Observed Fractures: depth & brief description
6.69-7.25	Zone I	this is a thick zone I, at top of an undulatory growth mound large relict cockscomb structures now halite	6.95: possible fracture at core break 7.05: infilled fracture
7.25-7.41	Zone II	undulatory, in some places, chaotic halite laminae	7.41: possible infilled fracture
7.41-7.48	Zone III	(note: zone is relatively thin)	
7.48-7.5	Zone IV	(note: zone is relatively thin)	
7.5	Zone IV	partial core	

WIPP Core Description Room C1, Borehole C1X05
Marker Bed 140
Depth of top/bottom contacts, m/ft: 23.1-27.14m / 77.4-89.0'
Date: July 8, 1994

Interval m.	Marker Bed Zone from Borns (1985)	Description:	Observed Fractures: depth & brief description
22.8 - 23.25	I-II?	nodular anhydrite in secondary matrix of polyhalite, anhydrite and halite (?)	possible fracture healed @ 22.85
23.25 - 24.10	III	laminated anhydrite with <5mm tubular halite after gypsum, 2-4cm horizontal zones of halite after gypsum (swallow tail) @ 23.7, 24.0, 24.05, 24.10	possible bedding plane fracture @ 24.05
24.20 24.32	III?	swallow tail gypsum replaced by halite in anhydrite matrix	
24.32 - 24.42	III?	possible breccia of anhydrite and gypsum replaced by halite (halite partially removed)	
24.43 25.15	IV	massive gray laminated anhydrite, numerous bedding planes, horizontal crystal breccias @ 24.45, 24.47	possible bedding plane fracture @ 24.55, 24.6, 25.15
25.15 26.30	II?	massive gray anhydrite, convolute bedding, local polyhalite and halite overprint @ 25.32, 25.55	
26.30 26.50	V	clay with anhydrite and halite	
26.50 - 27.1	IV	laminated anhydrite may be clastic 26.5-26.6	numerous bedding planes for fractures
27.1 end	V	basal gray clay with halite and anhydrite	

WIPP Core Description Room C1, Borehole C1X06
Marker Bed 139
Depth of top/bottom contacts, m/ft: 6.43-7.32m / 21.1-24.0'
Date: June 10, 1994

Interval m.	Marker Bed Zone from Borns (1985)	Description:	Observed Fractures: depth & brief description
6.43-6.65	Zone I	relict chevron growths large halite patch crystal breecia @ 6.6	6.43: possible infilled fracture at contact
6.65-6.71	Zone II	gray anhydrite undulatory and in places chaotic	
6.71-7.1	Zone III	relict swallow tails halite-rich layers 6.9 to 7.1 varying dips relative to core	6.71: infilled fracture 6.72: infilled fracture 6.83: core break 7.1: infilled fracture
7.1-7.25	Zone IV	gray laminated anhydrite	7.13: infilled fracture
7.25-7-4	Zone IV	poor core recovery	
7.4	Zone V	basal clay	

WIPP Core Description Room C1, Borehole C1X06
Marker Bed 140
Depth of top/bottom contacts, m/ft: 22.96-27.14m / 75.7-89.0'
Date: July 11, 1994

Interval m.	Marker Bed Zone from Borns (1985)	Description:	Observed Fractures: depth & brief description
22.9 to 23.0	I	dipping, halite crystal mound	inclined stylolite or infilled fracture at upper contact
23.0 to 23.5	II (poor core recovery)	convolute anhydrite laminae with halite	
23.5 to 24.2	III	(poor core recovery) laminated anhydrite characterized by swallow tail growths, gypsum replaced by halite	difficult to place fractures with amount of core break up
24.2 to 25.5	IV	massive gray anhydrite, weakly laminated, possible stylolytic growths	no apparent fractures section or core seems very competent
25.5 to 25.7	IV	gray-brown anhydrite wavy interfaces between layers	core competent
25.7 to 26.0	IV	halite-polyhalite overprinting original laminated fabric	possible fracture @ core break 25.83
26.05 to 26.22	II-III	laminated anhydrite (brown/gray) with polyhalite-halite, layers dip	possible fracture @ 26.18 @ core break
26.22 to 26.30		clay seam (gray)	
26.30 to 26.40	IV	massive gray anhydrite	core disks, possible preserved fracture @ 26.4
26.40 to 27.0	IV	massive gray anhydrite	less disking, possible infilled fractures @ 26.59, 26.58, 26.57

WIPP Core Description Room C1, Borehole C1X10
Marker Bed 139
Depth of top/bottom contacts, m/ft: 7.51-8.26m / 24.6-27.1'
Date: June 9, 1994

Interval m.	Marker Bed Zone from Borns (1985)	Description:	Observed Fractures: depth & brief description
	Zone I not observed	core loss?	
7.51-7.75	Zone II	halite pseudomorphs after gypsum	7.58: filled fracture? 7.65: filled bedding plane fracture at core break 7.72: filled bedding plane fracture
7/75-7.8	Zone III	massive gray anhydrite with patches of halite, pseudomorphs after gypsum	7.75: core break possible traces of subvertical fracture 7.29: subvertical fracture
7.8 - core break	Zone IV	massive gray anhydrite large halite pseudomorphs after gypsum	7.87: bedding plane fracture 7.88: bedding plane fracture
lost core			

WIPP Core Description Room C1, Borehole C1H05
Marker Bed 139
Depth of top/bottom contacts, m/ft: 7.13-7.90m/23.4-25.9'
Date: June 10, 1994

Interval m.	Marker Bed Zone from Borns (1985)	Description:	Observed Fractures: depth & brief description
7.13-7.15	Zone I	thin zone of crystal breccia	
7.15-7.19	? core loss		
7.19-7.31	Zone II	little polyhalite, tabular halite after gypsum	7.19: bedding plane fracture 7.31: bedding plane fracture 7.24: filled fracture
7.31-7.65	Zone III	gray anhydrite with layers of halite, pseudomorphs after gypsum	7.35: bedding plane fracture 7.60: bedding plane fracture 7.65: bedding plane fracture
7.65-7.9	Zone IV	massive gray anhydrite (photo blurred difficult to pick fractures)	7.75: core break 7.85: core break 7.87: core break 7.89: core break 7.91: core break
7.9	Zone V	not observed. Clay may have been lost during drilling.	

WIPP Core Description Room C1, Borehole C1H06
Marker Bed 139
Note: Core direction dips 70° from horizontal
Depth of top/bottom contacts, m/ft: 8.4-9.6m inclined ; 7.9-8.5m vertical / 25.9-27.9'
Date: June 9, 1994

Interval m.	Marker Bed Zone from Borns (1985)	Description:	Observed Fractures: depth & brief description
8.2-8.3*	Zone I	undulatory contact zone	possible infilled fracture at contact
8.3-8.45	Zone II	polyhalitic overprint; stylolitic band, milky white fracture infilling	8.35: stylolite or possible infilled fracture 8.4: stylolite or possible infilled fracture 8.42: stylolite or possible fracture
8.5-8.6	Zone III	gray anhydrite with halite layers, pseudomorphs after gypsum	8.5: core break
8.6-9.0	Zone IV	gray anhydrite laminated, relict bedding structure @ 8.65: polyhalitic replacement along bedding-plane fracture	8.6: core break 8.8: bedding plane fracture 8.89: core break along bedding plane fracture
8.92	Zone V only partial recovery		8.97: core break

*7.31-7.39m projected vertical distance

WIPP Core Description Room C1, Borehole C1H07
Marker Bed 139
Depth of top/bottom contacts, m/ft: 6.77-7.70m / 22.2-24.7'
Date: June 10, 1994

Interval m.	Marker Bed Zone from Borns (1985)	Description:	Observed Fractures: depth & brief description
6.78-6.9	Zone I	crystal breccia, halite replacing gypsum	6.9: core break
6.9-7.1	Zone II	gray anhydrite layers marked by halite pseudomorphs after gypsum, in places deformed and chaotic	7.09: core break
7.1-7.4	Zone III	Layered gray anhydrite	7.4: core break
7.53	core loss		

WIPP Core Description Room C1, Borehole C1H07
Marker Bed 140
Depth of top/bottom contacts, m/ft: 22.8-27.23m / 74.8-89.3'
Date: July 8, 1994

Interval m.	Marker Bed Zone from Borns (1985)	Description:	Observed Fractures: depth & brief description
22.75 22.81	I-II	upper contact growth structures, anhydrite and halite mixture	
22.81 - 23.60	II, III	anhydrite with polyhalitic and halitic overprinting, inclined contorted bedding	core disks more than C1X05 habit of fractures similar to preexisting fractures in MB139
23.60 - 25.20	IV	weakly laminated massive gray anhydrite, tabular swallow tail gypsum replaced by halite @ 23.6, 23.70, 23.80-24.20	core disks frequently from 24.20-24.90 appears again similar to partially filled fractures in MB139
25.20 - 26.40	?	massive gray anhydrite overprinted by secondary halite, anhydrite and polyhalite overprint forms mesh over relict anhydrite	partially open fracture @ 25.82, 25.88, 26.4
26.4 - 26.7	V	gray clay, anhydrite halite, inclined contact	
26.7 - 27.2	IV	gray massive anhydrite, laminae of halite after gypsum @ 26.8	bedding plane fracture @ 26.85 disking between 26.7 - 26.8
27.2 - end	V	basal gray clay	

Appendix C - Schematics of Hydraulic Fracturing Tools

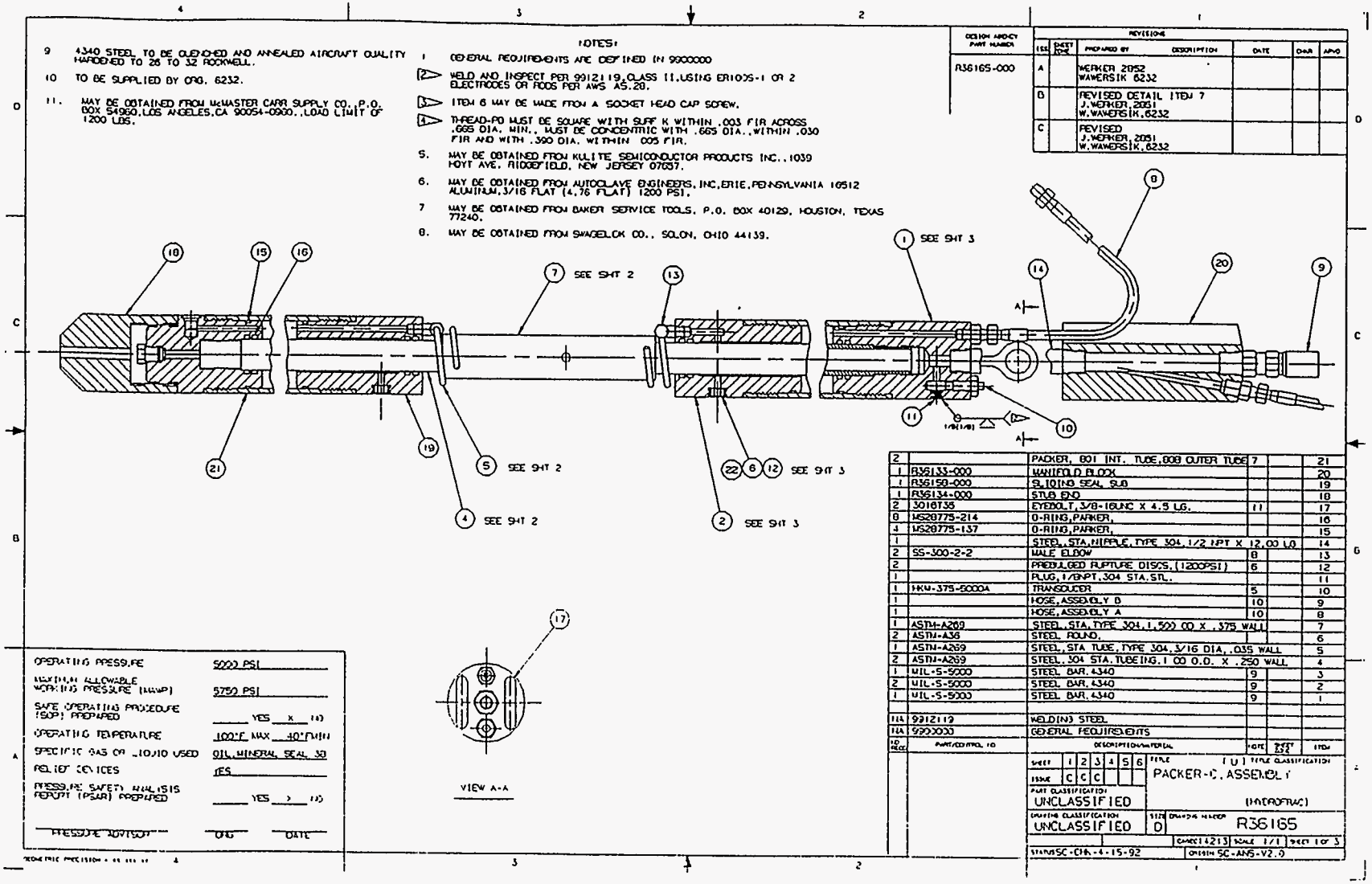

Figure C1 - Assembly drawing of single-zone, 2-packer systems used for hydraulic fracturing tests in MB139.

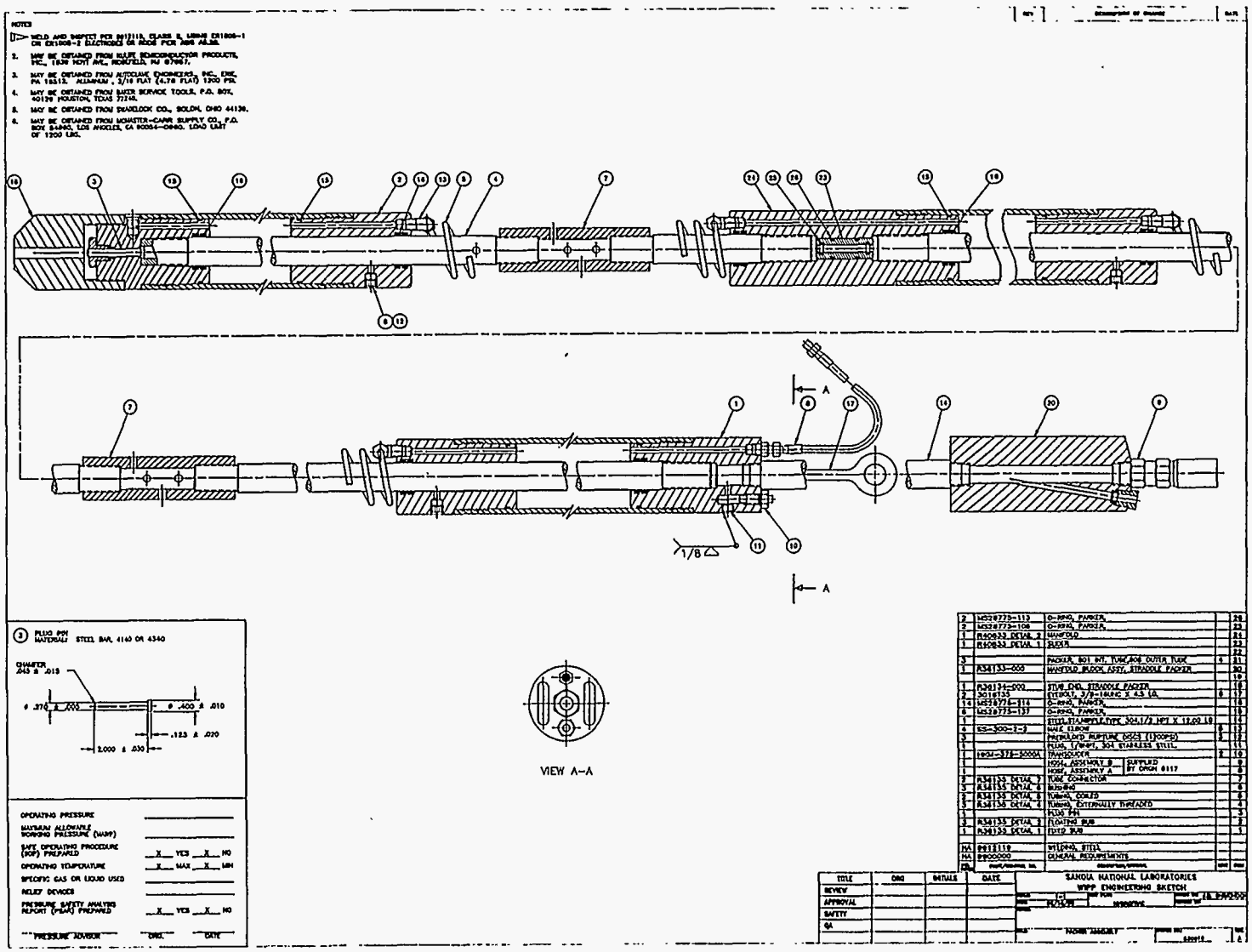

Figure C2 - Assembly drawing of two-zone, 3-packer systems used for hydraulic fracturing tests in MB140.

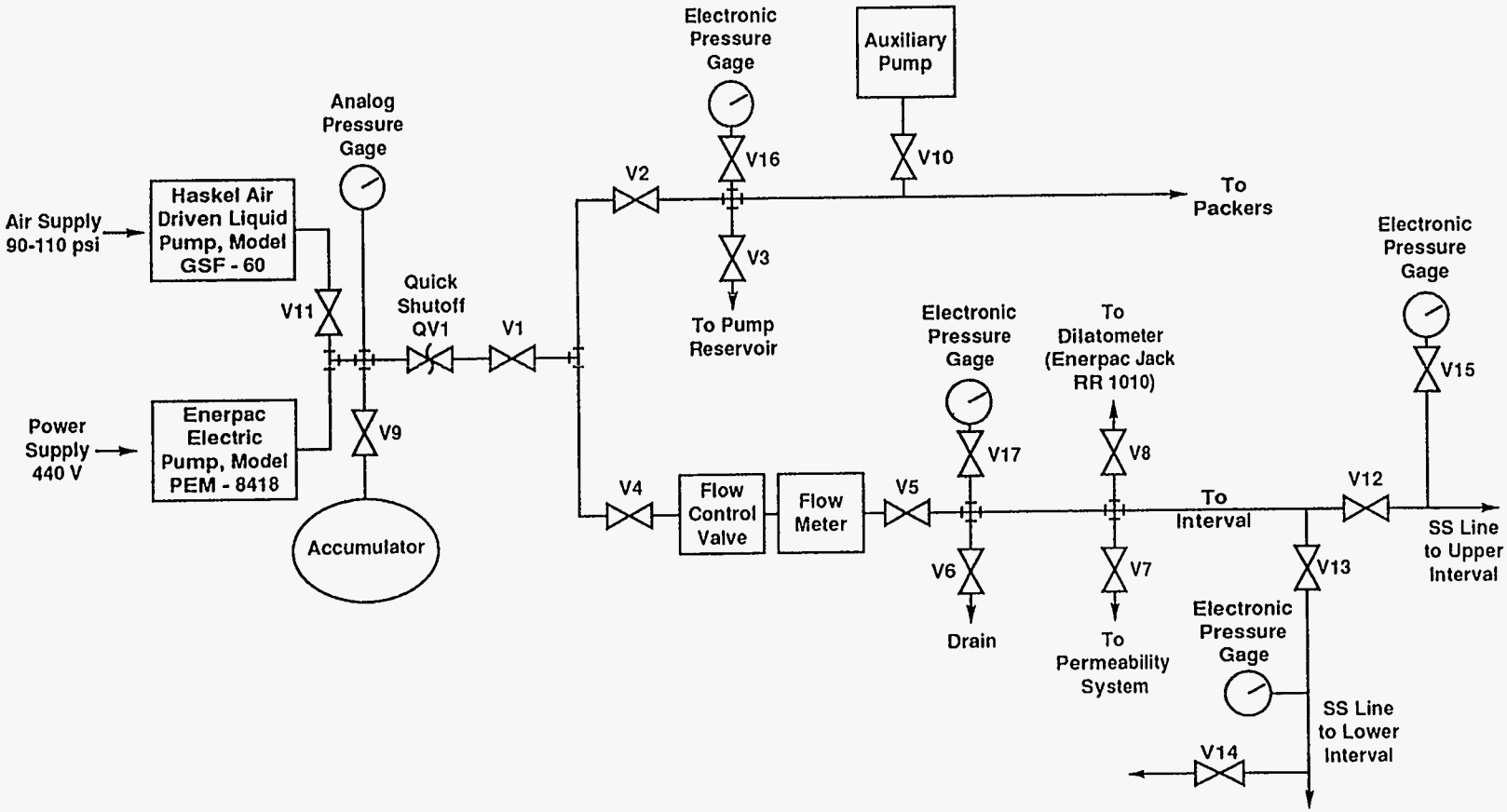

Figure C3 - Schematic of system plumbing for hydraulic fracturing tests in Room C1.

Appendix D - System Compliance Data

The packer and interval compliances were measured for both types of straddle packers shown in Figures C1 and C2. The tests were completed either in a four-inch-diameter steel pipe or downhole as indicated below. In all cases, pressure was changed by means of a construction type hydraulic hand pump (Enerpac, model P84). The fluid volumes injected or withdrawn were determined from the ram travel of a dual-acting hydraulic actuator (Enerpac, model RR1010) with known cross-sectional area (4.85 cm^2). Linear ram travel was read off a millimeter scale and wire marker that were attached to the moving ram and actuator body, respectively. This relatively crude method was first used during hydraulic fracturing stress measurements in the WIPP in 1985 with surprisingly consistent results.

Single-Zone (2-Packer) Straddle Packer (Figure C1) - Packer Compliance Test in Steel Pipe Without Accumulator

Date of test: 8/15/91
Test Location: 4-inch-diameter steel pipe
Packer supply line: 50-ft (15.2-m) hydraulic hose
Interval supply line: 50-ft (15.2-m) stainless steel tubing, I.D.=0.305 in (0.775 cm)
Packer pressure during test: see table below
Interval pressure during test: atmospheric

Table D.1 - Packer pressure, p_p, and linear dilatometer travel, d.

p_p psi	d cm
Test 1	
656	5.3
709	5.7
1005	8.4
1106	9.4
1250	10.7
1350	11.55
1510	13.
1611	13.9

p_p psi	d cm
Test 2	
1715	1.4
1876	2.7
2058	4.2
2302	6.5
2413	7.4
2437	7.4
2577	8.35
2725	9.5

Inferred compliances (2 packers): 44.0 and 41.3 cc/1000 psi (6.381 and 5.99 cc/MPa)

Note: during hydrologic testing the packer pressure was maintained constant by means of a 5-gal accumulator. Sixty to seventy-five percent of the accumulator volume was occupied by gas. Based on downhole measurements in MB140, the packer compliance with the accumulator on line was approximately 60 times lower than without the accumulator.

Single-Zone (2-Packer) Straddle Packer (Figure C1) - Interval Compliance Test in Steel Pipe

Date of test: 8/15/91
Test Location: 4-inch-diameter steel pipe
Packer supply line: 50-ft (15.2-m) hydraulic hose
Interval supply line: 50-ft (15.2-m) stainless steel tubing, I.D.= I.D.=0.305 in (0.775 cm)
Packer pressure during test: 1900 psi (13.1 MPa)
Interval pressure during test: see table below

Table D.2 - Interval pressure, p_s, and linear dilatometer travel, d.

p_s psi	d cm
451	5.5
650	6.4
733	6.8
885	7.55
991	8
1090	8.55

Inferred compliance: 23.3 cc/1000 psi (3.38 cc/MPa).

Single-Zone (2-Packer) Straddle Packer (Figure C1) - Compliance Test Downhole

Date of test: 7/1/92
Test Location: MB139 in borehole C1X10
Packer supply line: 50-ft (15.2-m) hydraulic hose
Interval supply line: 50-ft (15.2-m) stainless steel tubing, I.D.=0.305 in (0.775 cm)
Packer pressure during test: 1900 psi (13.1 MPa)
Interval pressure during test: see table below

Table D.3 - Interval pressure, p_s, and linear dilatometer travel, d.

p_s psi	d cm
103	6.9
156	7.3
179	7.5
205	7.7
225	7.9
252	8.1

Inferred compliance: 24.0 cc/1000 psi (3.48 cc/MPa).

Two-Zone (3-packer) Straddle Packer (Figure C2) - Packer Compliance Test Downhole Without Accumulator

Date of test: 6/2/93
Test Location: MB140 in borehole C1X05
Packer supply line: 75-ft stainless steel tubing
Interval supply line: 75-ft stainless steel tubing, I.D.=0.305 in (0.775 cm)
Packer pressure during test: see table below
Upper and lower interval pressures during test: 1895 psi (13.07 MPa)

Table D.4 - Packer pressure, p_p, and linear dilatometer travel, d.

p_p psi	d cm
1895	9.3
1961	10.2
1999	10.8
1995	10.8
1950	9.0
1893	9.6
1978	10.6
2006	11.1
2003	11.1
1906	10.2
1895	8.5
1973	10.5
2003	11.0
2002	10.1
1907	8.7

Inferred compliance: 66.7 cc/1000 psi (9.67 cc/MPa).

Note: during hydrologic testing the packer pressure was maintained constant by means of a 5-gal accumulator. Sixty to seventy-five percent of the accumulator volume was occupied by gas. Based on additional measurements, the packer compliance with the accumulator on line was approximately 60 times lower than without the accumulator.

Two-Zone (3-packer) Straddle Packer (Figure C2) - Upper Interval Compliance Test Downhole

Date of test: 6/2/93
Test Location: MB140 in borehole C1X05
Packer supply line: 75-ft (22.9-m) hydraulic hose
Interval supply lines: 75-ft (22.9-m) stainless steel tubing
Packer pressure during test: 1900 (13.1 MPa)
Upper interval pressure during test: see table below
Lower interval pressure: 1550 psi (10.69 MPa)

Table D.5 - Upper interval pressure, p_{su}, and linear dilatometer travel, d.

p_{su} psi	d cm
1551	8.75
1610	9.3
1702	10.1
1688	9.3
1501	7.9
1521	8.7
1628	9.35
1701	10.1

Inferred compliance (3-packers): 37.9 cc/1000 psi (5.50 cc/MPa)

Two-Zone (3-Packer) Straddle Packer (Figure C2) - Lower Interval Compliance Test Downhole

Date of test: 6/22/93
Test Location: MB140 in borehole C1X05
Packer supply line: 75-ft (22.9-m) hydraulic hose
Interval supply lines: 75-ft (22.9-m) stainless steel tubing, I.D.=0.305 in (0.775 cm)
Packer pressure during test: 1900 (13.1 MPa)
Upper interval pressure during test: 1895 (13.07 MPa)
Lower interval pressure: see table below

Table D.6 Lower interval pressure, p_{sl}, and linear dilatometer travel, d.

p_{sl} psi	d cm
1525	9.8
1593	10.8
1700	12.9
1697	12.2
1510	8.7
1540	9.8
1613	11.0
1701	12.9
1693	12.4
1459	8.0

Inferred compliance: 93.9 cc/1000 psi (13.62 CC/MPa)

Two-Zone (3-Packer) Straddle Packer (Figure C2) - Combined Upper and Lower Interval Compliance Test Downhole

Date of test: 6/2/93
Test Location: MB140 in borehole C1X05
Packer supply line: 75-ft (22.9-m) hydraulic hose
Interval supply lines: 75-ft (22.9-m) stainless steel tubing, I.D.=0.305 in (0.8=775 cm)
Packer pressure during test: 1900 (13.1 MPa)
Upper interval pressure during test: see table below
Lower interval pressure: see table below

Table D.7 - Combined upper and lower interval pressure, p_s, and linear dilatometer travel , d.

p_s psi	d cm
1700	14.5
1708	14.5
13.9	1681
1500	9.0

Inferred compliance: 131.6 cc/1000 psi (19.09 cc/MPa).

Appendix E - Instrumentation and Calibration Data

The instrumentation and calibrations applicable to hydraulic fracturing tests in Room C1 are listed below.

Borehole C1X10, MB139

Packer pressure gage: Kulite S/N 9104417
Conditioner/readout: Entran S/N 91070011
Gage isolation valve no.: V16
Calibration date (mo/yr): 6/91

Interval pressure gage in console: Kulite S/N 9104393
Conditioner/readout: Entran S/N 91070023
Gage isolation valve no.: V17
Calibration date (mo/yr): 6/91

Interval pressure gage downhole: Kulite S/N 9104414
Conditioner/readout: Entran S/N 91070020
Gage isolation valve no.: V12
Calibration date (mo/yr): 6/91

Borehole C1X05, MB139

Packer pressure gage in console: Kulite S/N 9104417
Conditioner/readout: S/N 91070011
Gage isolation valve no.: V16
Calibration date (mo/yr): 5/92

Interval pressure gage in console: Kulite S/N 4284-7-184
Conditioner/readout: Entran S/N 91070023
Gage isolation valve no.: V17
Calibration date (mo/yr): 5/92

Interval pressure gage downhole: Kulite S/N 4284-7-186
Conditioner/readout: Entran 91070020
Gage isolation valve no.: V12
Calibration date (mo/yr): 5/92

Borehole C1X05, MB140

Packer pressure gage in console: Kulite S/N 9104417
Conditioner/readout: S/N 91070011
Gage isolation valve no.: V16
Calibration date (mo/yr): 5/93

Upper Interval pressure gage 1 in console: Kulite S/N 4284-7-184
Conditioner/readout: Entran S/N 91070023
Gage isolation valve no.: V17
Calibration date (mo/yr): 5/93

Upper Interval pressure gage 2 in console (replacement for failed downhole gage): Kulite S/N 4022-6-214
Conditioner/readout: Entran 91070020
Gage isolation valve no.: V15
Calibration date (mo/yr): 5/93

Lower interval pressure gage in console: Kulite S/N 4022-6-215
Conditioner/readout: Beckman S/N 9304289
Gage isolation valve no.: V13
Calibration date (mo/yr): 5/93

All transducer calibrations were carried out by means of a transfer standard consisting of a BLH pressure transducer, S/N 56718, in conjunction with a BLH transducer conditioner/readout, S/N 4513. The latter equipment was calibrated as a system in the Standards Laboratory at Sandia National Laboratories.

WIPP
UC721 - DISTRIBUTION LIST
SAND95-0596

Federal Agencies

US Department of Energy (4)
Office of Civilian Radioactive Waste Mgmt.
Attn: Deputy Director, RW-2
Acting Director, RW-10
Office of Human Resources & Admin.
Director, RW-30
Office of Program Mgmt. & Integ.
Director, RW-40
Office of Waste Accept., Stor., & Tran.
Forrestal Building
Washington, DC 20585

Attn: Project Director
Yucca Mountain Site Characterization Office
Director, RW-3
Office of Quality Assurance
P.O. Box 30307
Las Vegas, NV 89036-0307

US Department of Energy
Albuquerque Operations Office
Attn: National Atomic Museum Library
P.O. Box 5400
Albuquerque, NM 87185-5400

US Department of Energy
Research & Waste Management Division
Attn: Director
P.O. Box E
Oak Ridge, TN 37831

US Department of Energy (5)
Carlsbad Area Office
Attn: G. Dials
D. Galbraith
M. McFadden
R. Lark
J. A. Mewhinney
P.O. Box 3090
Carlsbad, NM 88221-3090

US Department of Energy
Office of Environmental Restoration and
Waste Management
Attn: M Frei, EM-30
Forrestal Building
Washington, DC 20585-0002

US Department of Energy (3)
Office of Environmental Restoration and
Waste Management
Attn: J. Juri, EM-34, Trevion II
Washington, DC 20585-0002

US Department of Energy
Office of Environmental Restoration and
Waste Management
Attn: S. Schneider, EM-342, Trevion II
Washington, DC 20585-0002

US Department of Energy (2)
Office of Environment, Safety & Health
Attn: C. Borgstrom, EH-25
R. Pelletier, EH-231
Washington, DC 20585

US Department of Energy (2)
Idaho Operations Office
Fuel Processing & Waste Mgmt. Division
785 DOE Place
Idaho Falls, ID 83402

US Environmental Protection Agency (2)
Radiation Protection Programs
Attn: M. Oge
ANR-460
Washington, DC 20460

Boards

Defense Nuclear Facilities Safety Board
Attn: D. Winters
625 Indiana Ave. NW, Suite 700
Washington, DC 20004

Nuclear Waste Technical Review Board (2)
Attn: Chairman
J. L. Cohon
1100 Wilson Blvd., Suite 910
Arlington, VA 22209-2297

State Agencies

Attorney General of New Mexico
P.O. Drawer 1508
Santa Fe, NM 87504-1508

Environmental Evaluation Group (3)
Attn: Library
7007 Wyoming NE
Suite F-2
Albuquerque, NM 87109

NM Energy, Minerals, and Natural
Resources Department
Attn: Library
2040 S. Pacheco
Santa Fe, NM 87505

NM Environment Department (3)
Secretary of the Environment
Attn: Mark Weidler
1190 St. Francis Drive
Santa Fe, NM 87503-0968

NM Bureau of Mines & Mineral Resources
Socorro, NM 87801

Laboratories/Corporations

Battelle Pacific Northwest Laboratories
Battelle Blvd.
Richland, WA 99352

Los Alamos National Laboratory
Attn: B. Erdal, INC-12
P.O. Box 1663
Los Alamos, NM 87544

Southwest Research Institute (2)
Center for Nuclear Waste Regulatory Analysis
Attn: P. K. Nair
6220 Culebra Rd.
San Antonio, TX 78228-0510

Tech Reps, Inc. (3)
Attn: J. Chapman (1)
Loretta Robledo (2)
5000 Marble NE, Suite 222
Albuquerque, NM 87110

Westinghouse Electric Corporation (5)
Attn: Library
J. Epstein
J. Lee
B. A. Howard
R. Kehrman
P.O. Box 2078
Carlsbad, NM 88221

S. Cohen & Associates
Attn: Bill Thurber
1355 Beverly Road
McLean, VA 22101

RE/SPEC (2)
Attn: C. L. Howard
4775 Indian School Road NE
Albuquerque, NM 87110

INTERA, Inc. (2)
Attn: R. M. Roberts
1650 University Blvd. NE Suite 300
Albuquerque, NM 87102

D. R. Knowles
British Nuclear Fuels, plc
Risley, Warrington, Cheshire WA3 6AS
1002607 UNITED KINGDOM

**National Academy of Sciences,
WIPP Panel**

Howard Adler
Oxyrase, Incorporated
7327 Oak Ridge Highway
Knoxville, TN 37931

Tom Kiess
Board of Radioactive Waste Management
GF456
2101 Constitution Ave.
Washington, DC 20418

Rodney C. Ewing
Department of Geology
University of New Mexico
Albuquerque, NM 87131

Charles Fairhurst
Department of Civil and Mineral Engineering
University of Minnesota
500 Pillsbury Dr. SE
Minneapolis, MN 55455-0220

B. John Garrick
PLG Incorporated
4590 MacArthur Blvd., Suite 400
Newport Beach, CA 92660-2027

Leonard F. Konikow
US Geological Survey
431 National Center
Reston, VA 22092

Carl A. Anderson, Director
Board of Radioactive Waste Management
National Research Council
HA 456
2101 Constitution Ave. NW
Washington, DC 20418

Christopher G. Whipple
ICF Kaiser Engineers
1800 Harrison St., 7th Floor
Oakland, CA 94612-3430

John O. Blomeke
720 Clubhouse Way
Knoxville, TN 37909

Sue B. Clark
University of Georgia
Savannah River Ecology Lab
P.O. Drawer E
Aiken, SC 29802

Konrad B. Krauskopf
Department of Geology
Stanford University
Stanford, CA 94305-2115

Della Roy
Pennsylvania State University
217 Materials Research Lab
Hastings Road
University Park, PA 16802

David A. Waite
CH_2 M Hill
P.O. Box 91500
Bellevue, WA 98009-2050

Thomas A. Zordon
Zordan Associates, Inc.
3807 Edinburg Drive
Murrysville, PA 15668

Jeremiah O'Driscoll
Jody Incorporated
505 Valley Hill Dr.
Atlanta, GA 30350

Universities

University of New Mexico
Geology Department
Attn: Library
141 Northrop Hall
Albuquerque, NM 87131

University of Washington
College of Ocean & Fishery Sciences
Attn: G. R. Heath
583 Henderson Hall, HN-15
Seattle, WA 98195

Libraries

Thomas Brannigan Library
Attn: D. Dresp
106 W. Hadley St.
Las Cruces, NM 88001

Government Publications Department
Zimmerman Library
University of New Mexico
Albuquerque, NM 87131

New Mexico Junior College
Pannell Library
Attn: R. Hill
Lovington Highway
Hobbs, NM 88240

New Mexico State Library
Attn: N. McCallan
325 Don Gaspar
Santa Fe, NM 87503

New Mexico Tech
Martin Speere Memorial Library
Campus Street
Socorro, NM 87810

WIPP Public Reading Room
Carlsbad Public Library
101 S. Halagueno St.
Carlsbad, NM 88220

Foreign Addresses

Atomic Energy of Canada, Ltd.
Whiteshell Laboratories
Attn: B. Goodwin
Pinawa, Manitoba, CANADA R0E 1L0

Francois Chenevier
ANDRA
Route de Panorama Robert Schumann
B. P. 38
92266 Fontenay-aux-Roses, Cedex
FRANCE

Claude Sombret
Centre d'Etudes Nucleaires de la Vallee Rhone
CEN/VALRHO
S.D.H.A. B.P. 171
30205 Bagnols-Sur-Ceze, FRANCE

Commissariat a L'Energie Atomique
Attn: D. Alexandre
Centre d'Etudes de Cadarache
13108 Saint Paul Lez Durance Cedex
FRANCE

Jean-Pierre Oliver
OECD Nuclear Energy Agency
DIV. of Radiation Protection and Waste Mgt.
38 Boulevard Suchet
75016 Paris, FRANCE

Bundesanstalt fur Geowissenschaften und Rohstoffe
Attn: M. Langer
Postfach 510 153
D-30631 Hannover, GERMANY

Bundesministerium fur Forschung und Technologie
Postfach 200 706
5300 Bonn 2, GERMANY

Institut fur Tieflagerung
Attn: K. Kuhn
Theodor-Heuss-Strasse 4
D-3300 Braunschweig, GERMANY

Gesellschaft fur Anlagen und Reaktorsicherheit (GRS)
Attn: B. Baltes
Schwertnergasse 1
D-50667 Cologne, GERMANY

Bundesanstalt fur Strahlenschutz
Attn: P. Brenneke
Postfach 100149
38201 Salzgitter 1
3300 Braunschweig, GERMANY

Studiecentrum Voor Kerenergie
Centre d'Energie Nucleaire
Attn: A. Bonne
SCK/CEN Boeretang 200
B-2400 Mol, BELGIUM

Shingo Tashiro
Japan Atomic Energy Research Institute
Tokai-Mura, Ibaraki-Ken, 319-11
JAPAN

Netherlands Energy Research Foundation ECN (2)
Attn: J. Prij
L. H. Vons
3 Westerduinweg
P.O. Box 1
1755 ZG Petten
THE NETHERLANDS

Svensk Karnbransleforsorjning AB
Attn: F. Karlsson
Project KBS (Karnbranslesakerhet)
Box 5864
S-102 48 Stockholm
SWEDEN

Nationale Genossenschaft fur die Lagerung Radioaktiver Abfalle (2)
Attn: S. Vomvoris
P. Zuidema
Hardstrasse 73
CH-5430 Wettingen
SWITZERLAND

AEA Technology
Attn: J. H. Rees
D5W/29 Culham Laboratory
Abington, Oxfordshire OX14 3DB
UNITED KINGDOM

AEA Technology
Attn: W. R. Rodwell
044/A31 Winfrith Technical Centre
Dorchester, Dorset DT2 8DH
UNITED KINGDOM

AEA Technology
Attn: J. E. Tinson
B4244 Harwell Laboratory
Didcot, Oxfordshire OX11 ORA
UNITED KINGDOM

Internal

MS	Org.	
1324	6115	P. B. Davies
1320	6831	E. J. Nowak
1322	6121	J. R. Tillerson
1328	6849	D. R. Anderson
1328	6848	H. N. Jow
1335	6801	M. Chu
1341	6832	J. T. Holmes
1395	6800	L. Shephard
1395	6821	M. Marietta
1395	6841	V. H. Slaboszewicz
1337	6000	W. D. Weart
1033	6111	J. A. Henfling
1324	6115	R. L. Beauheim (12)
0750	6116	D. J. Borns (5)
0751	6117	L. W. Carlson
0751	6117	W. R. Wawersik (12)
1395	6700	P. L. Jones
1395	6811	S. Y. Pickering
0841	9100	P. J. Hommert
1322	6121	L. D. Hurtado
1322	6121	F. D. Hansen
1322	6121	M. K. Knowles
0706	6113	D. E. Munson
0751	6117	L. S. Costin (5)
1330	6811	K. Hart (2)
1330	4415	NWM Library (20)
9018	8940-2	Central Technical Files
0899	4414	Technical Library (5)
0619	12690	Review and Approval Desk (2), For DOE/OSTI